Electronic Supplementary Material (ESI) for Soft Matter.

Electronic Supporting Information

S1. ^{1}H, ^{13}C and ^{11}B NMR spectra of new compounds

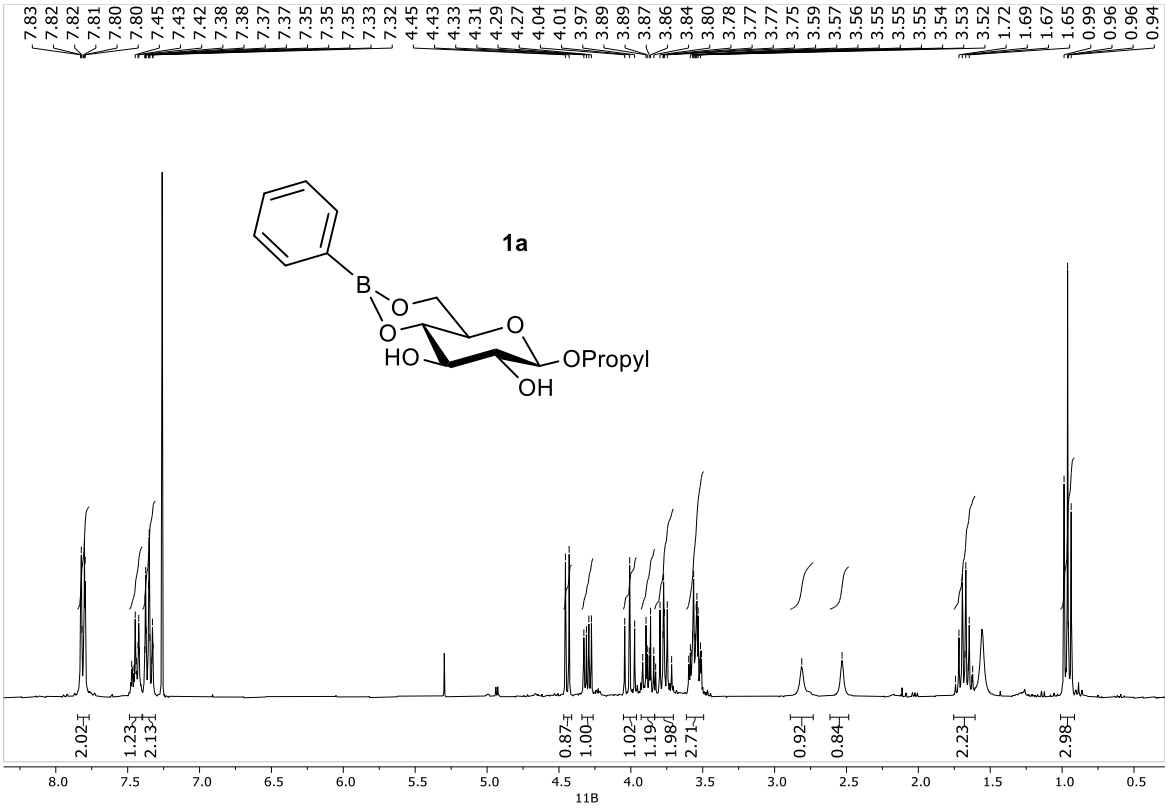

^{1}H NMR spectrum ($CDCl_3$, 300 MHz) of compound **1a**

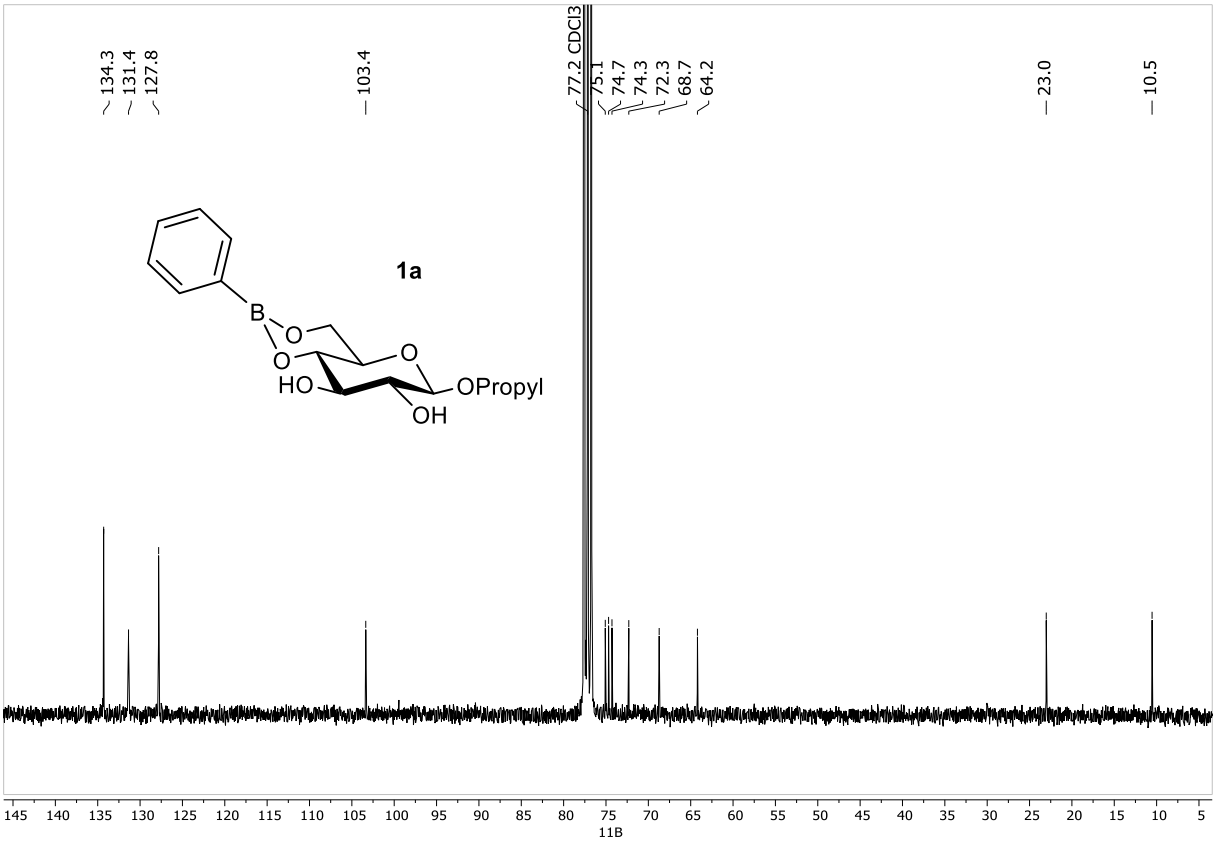

^{13}C NMR spectrum ($CDCl_3$, 75 MHz) of compound **1a**

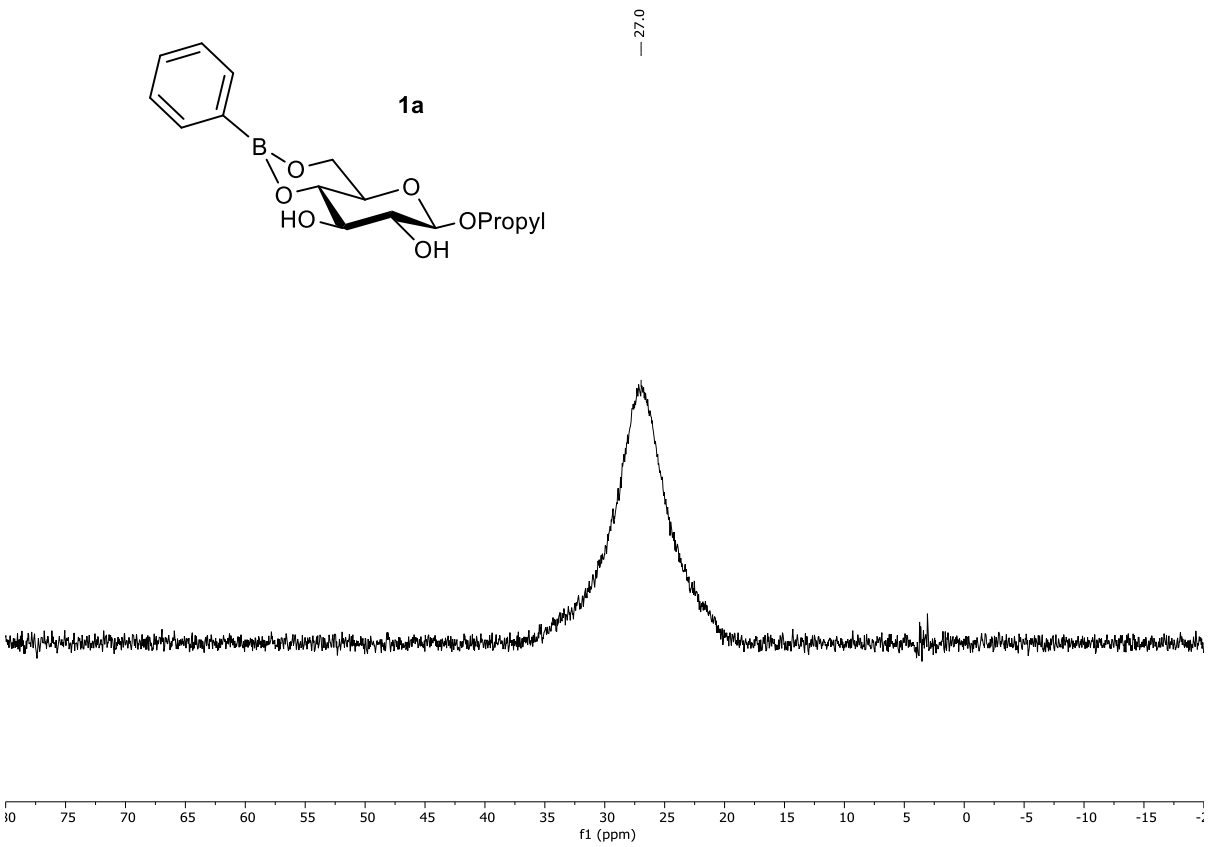

$^{11}B\{1H\}$ NMR ($CDCl_3$, 96 MHz) of compound **1a**

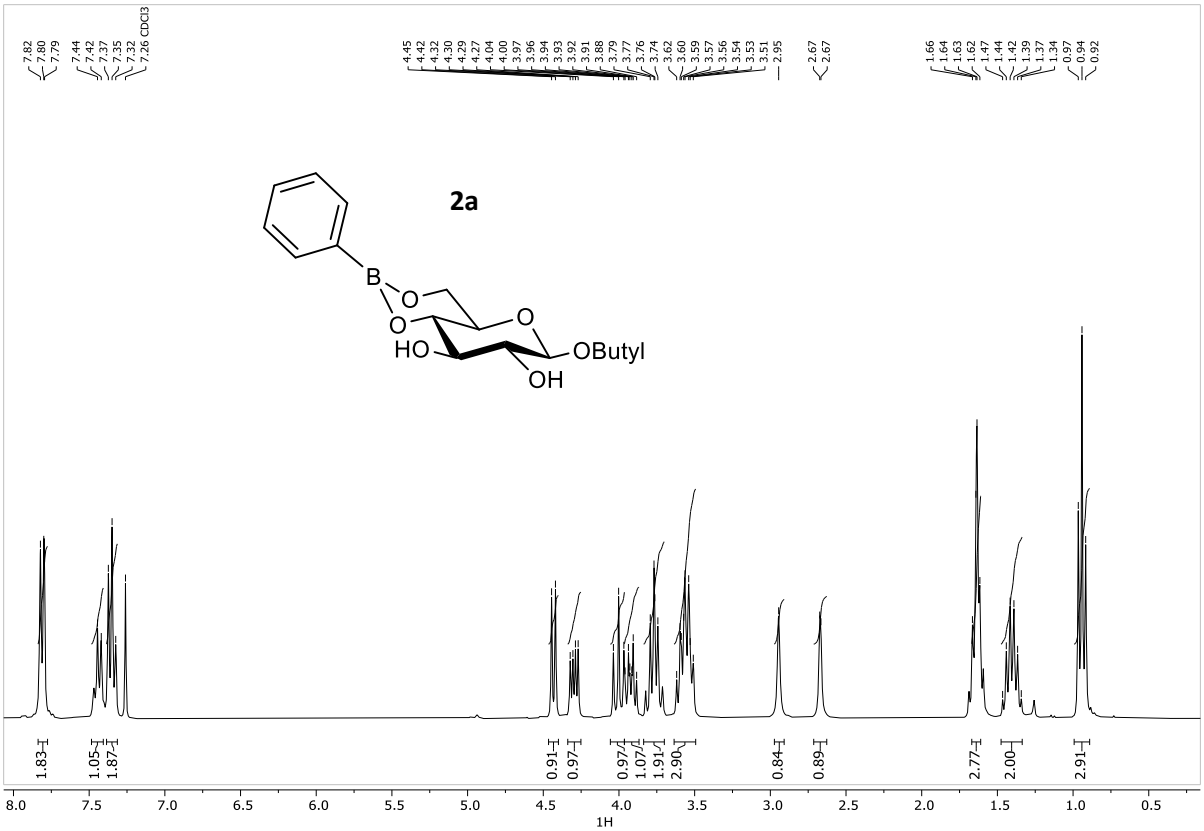

^{1}H NMR spectrum ($CDCl_3$, 300 MHz) of compound **2a**

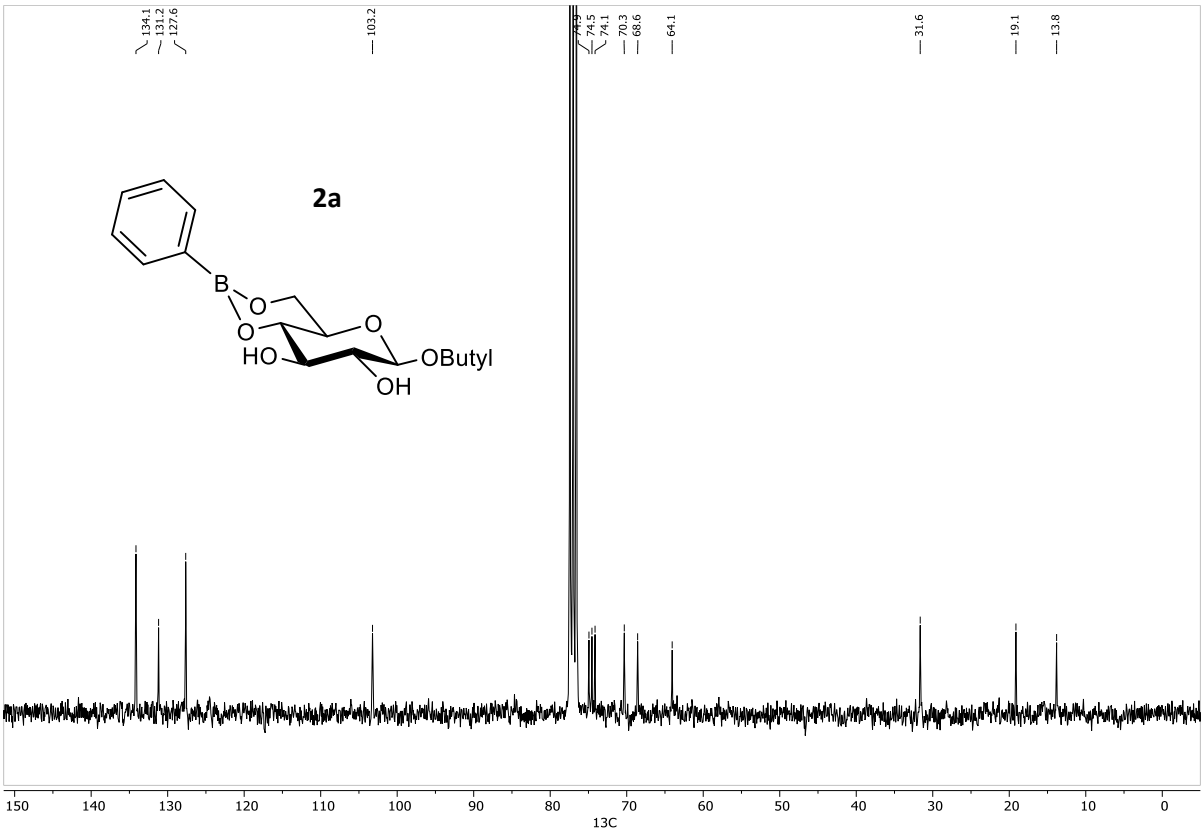

^{13}C NMR spectrum ($CDCl_3$, 75 MHz) of compound **2a**

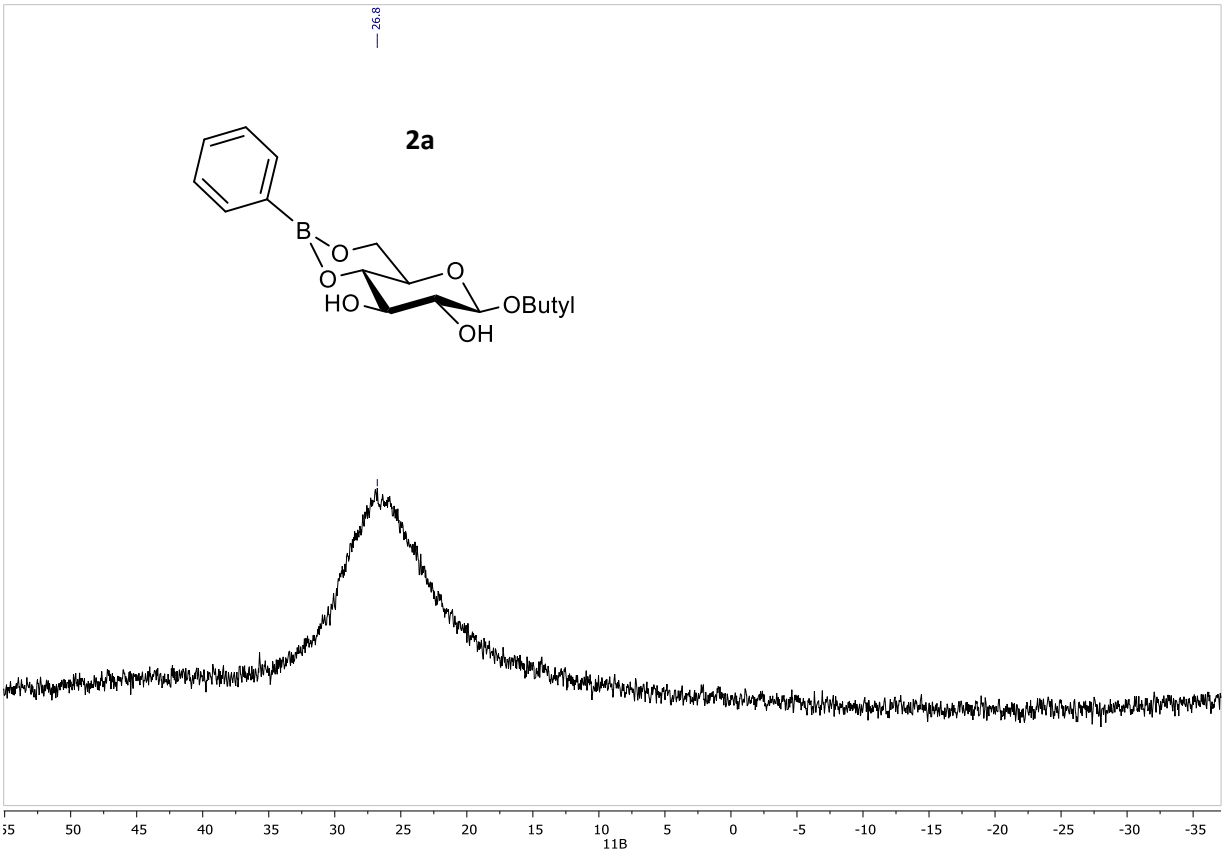

$^{11}B\{1H\}$ NMR ($CDCl_3$, 96 MHz) of compound **2a**

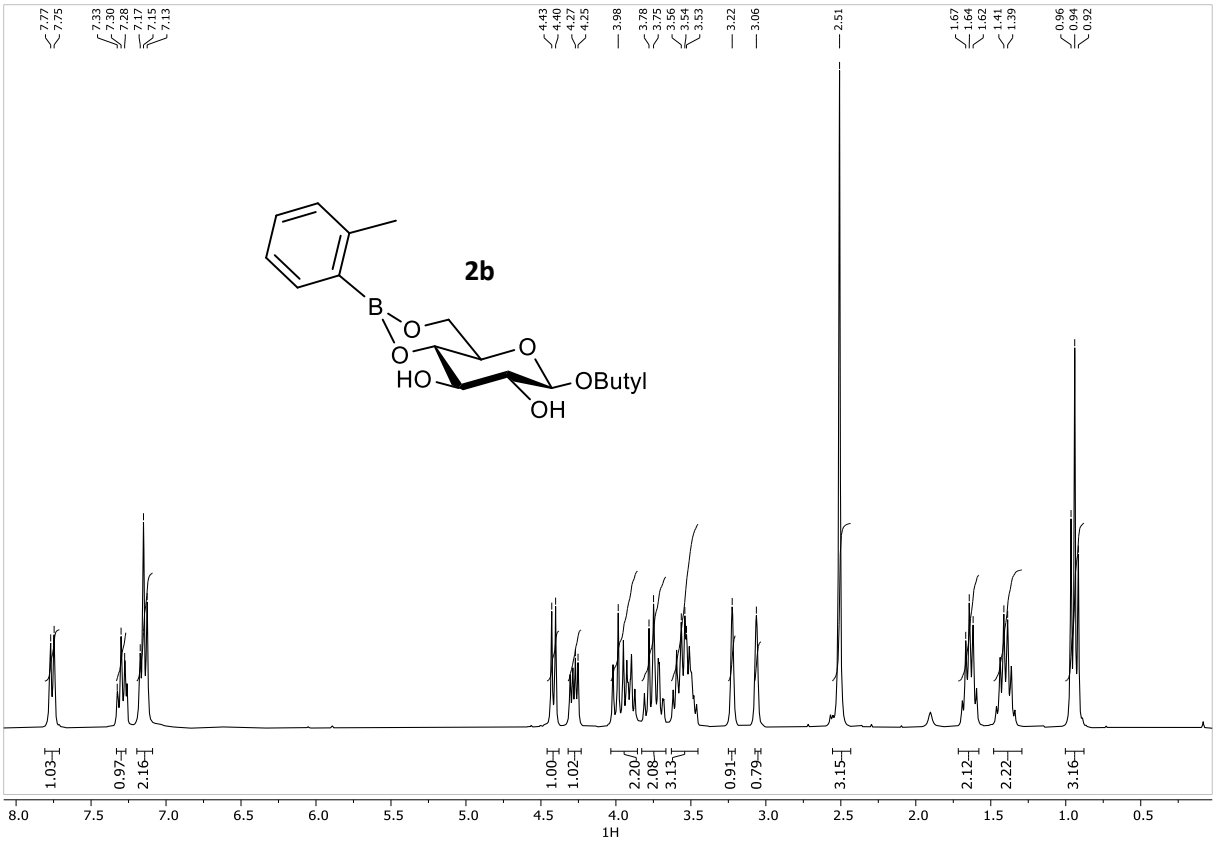

^{1}H NMR spectrum ($CDCl_3$, 300 MHz) of compound **2b**

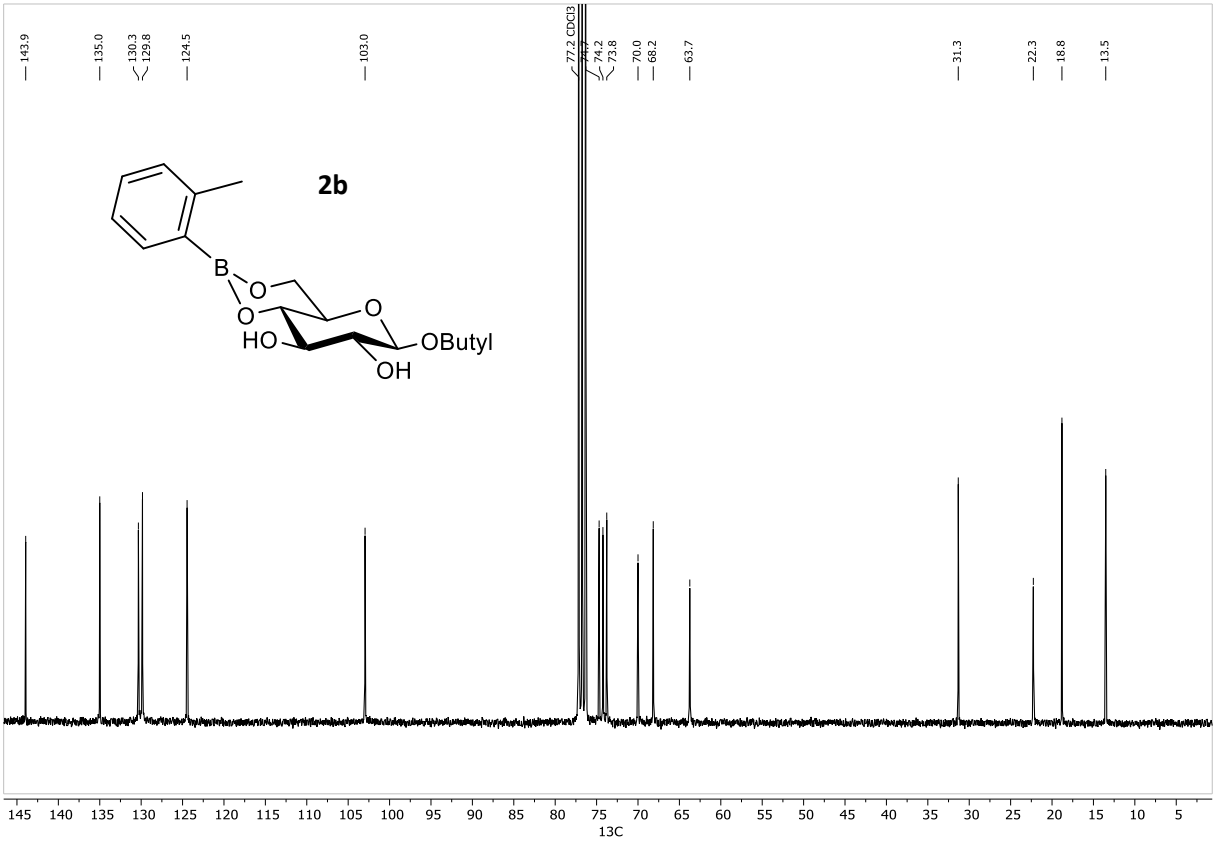

^{13}C NMR spectrum ($CDCl_3$, 75 MHz) of compound **2b**

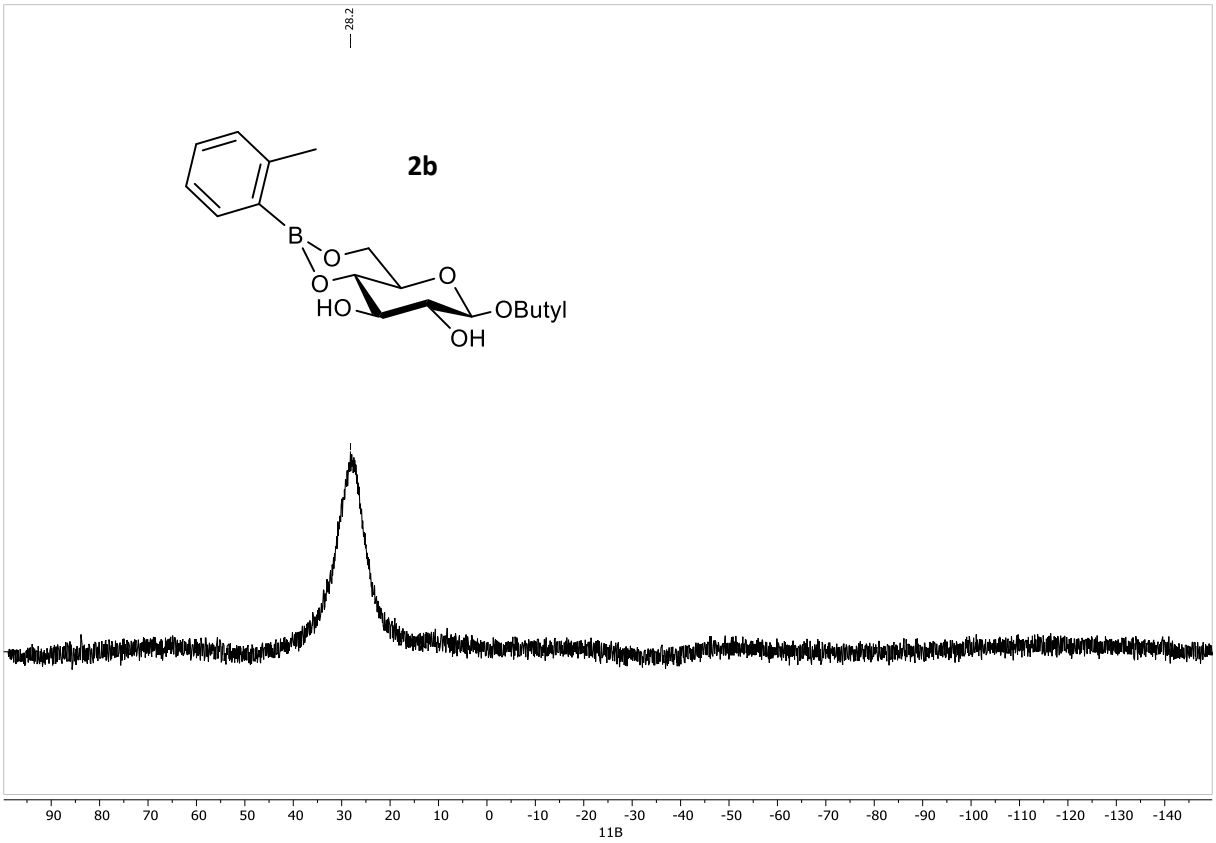

$^{11}B\{1H\}$ NMR ($CDCl_3$, 96 MHz) of compound **2b**

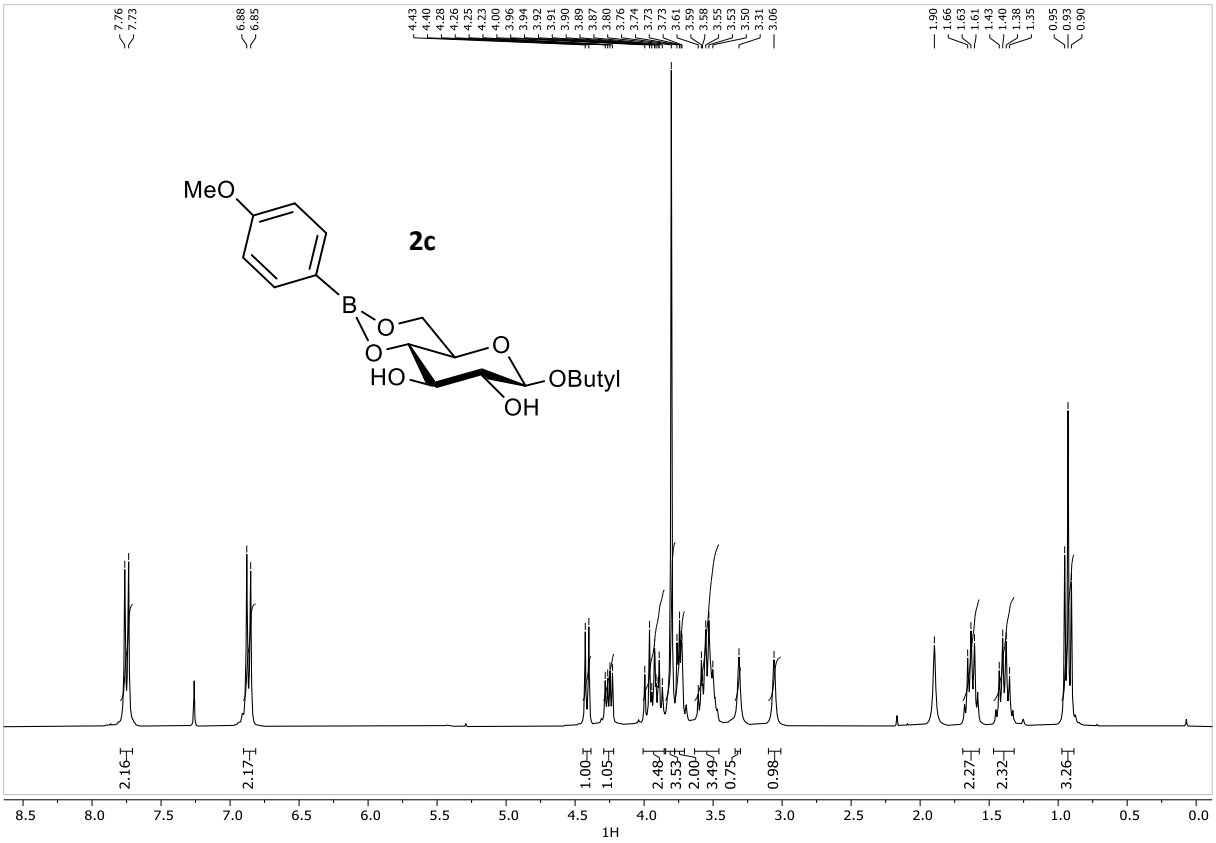

^{1}H NMR spectrum ($CDCl_3$, 300 MHz) of compound **2c**

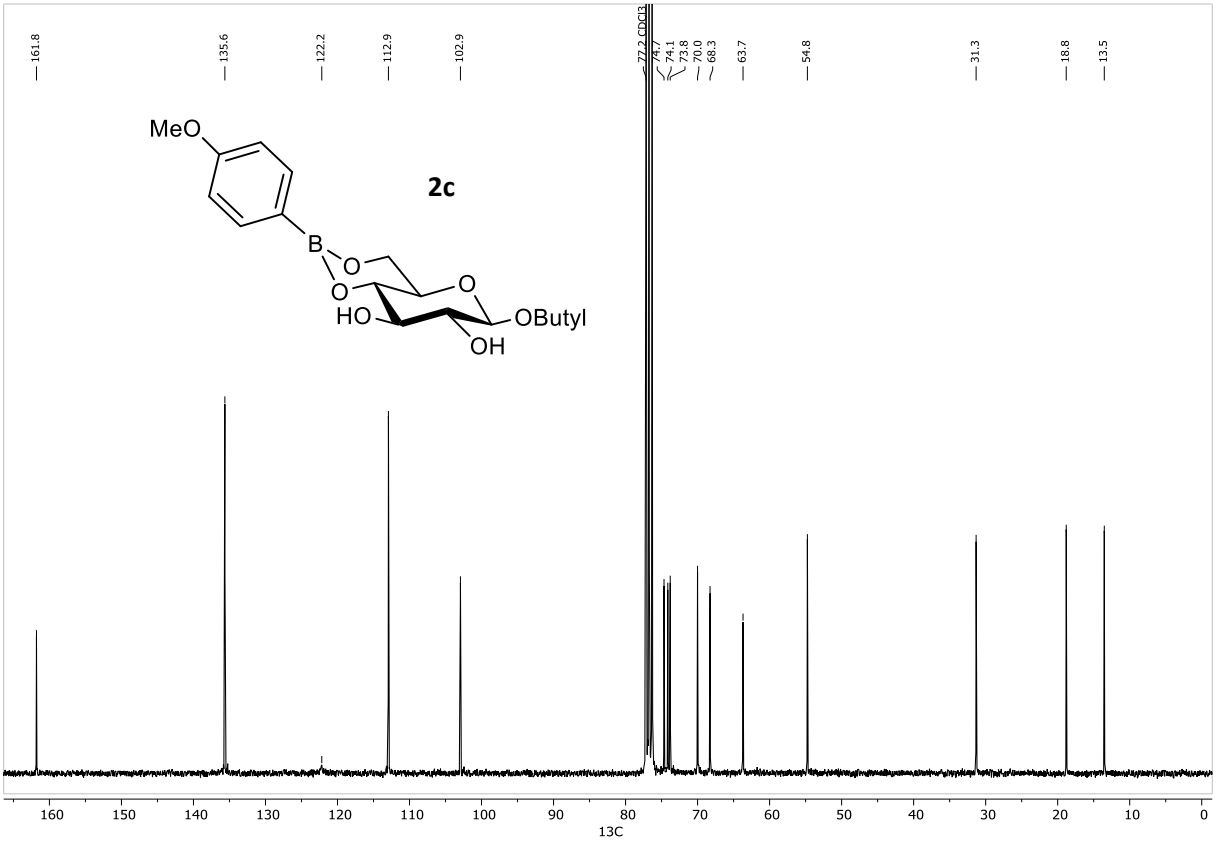

^{13}C NMR spectrum ($CDCl_3$, 75 MHz) of compound **2c**

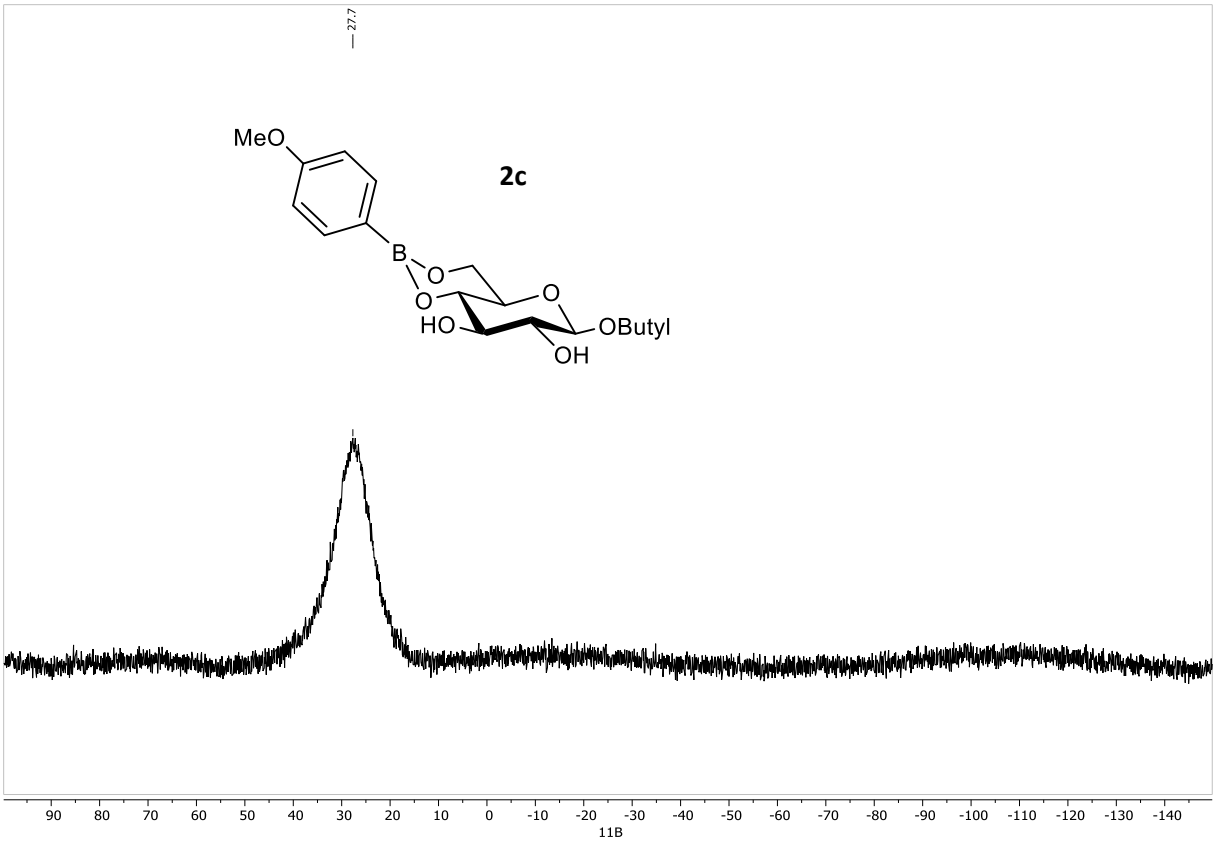

$^{11}B\{1H\}$ NMR ($CDCl_3$, 96 MHz) of compound **2c**

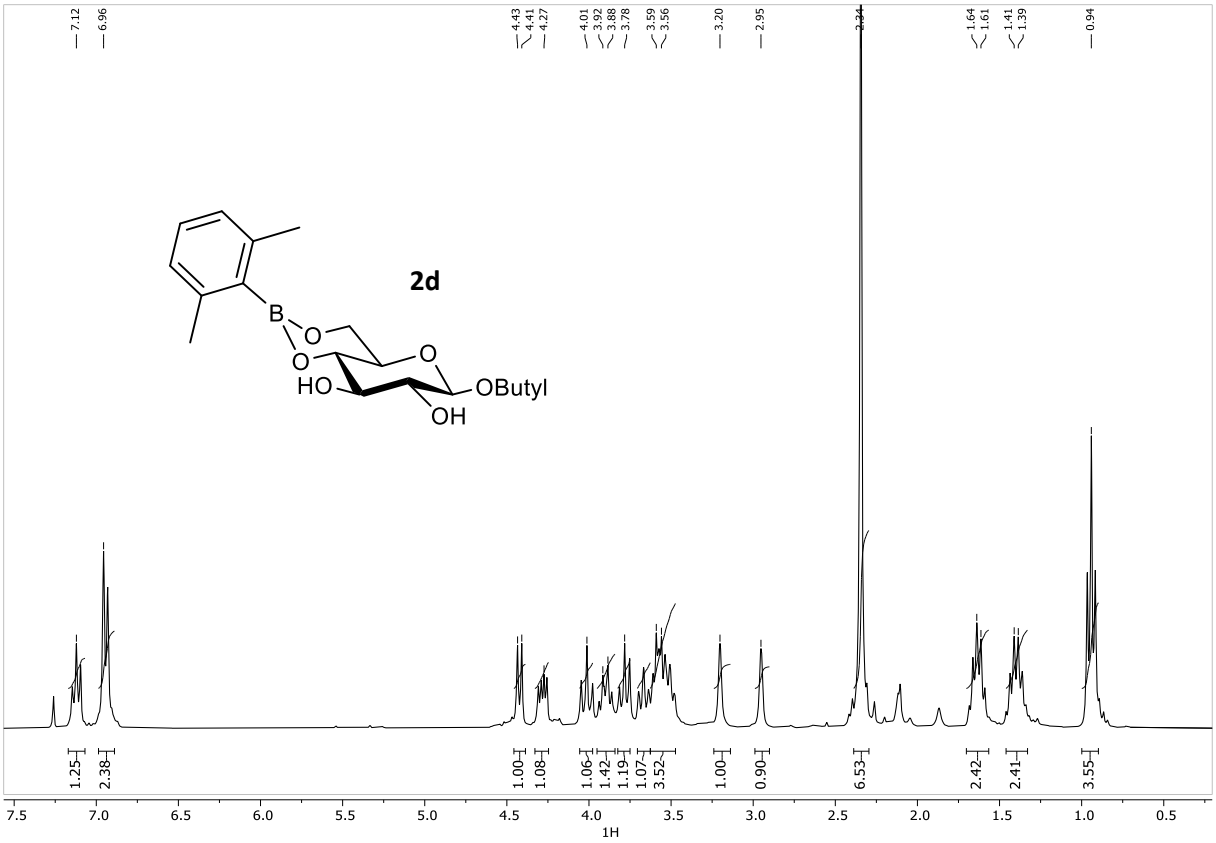

^{1}H NMR spectrum ($CDCl_3$, 300 MHz) of compound **2d**

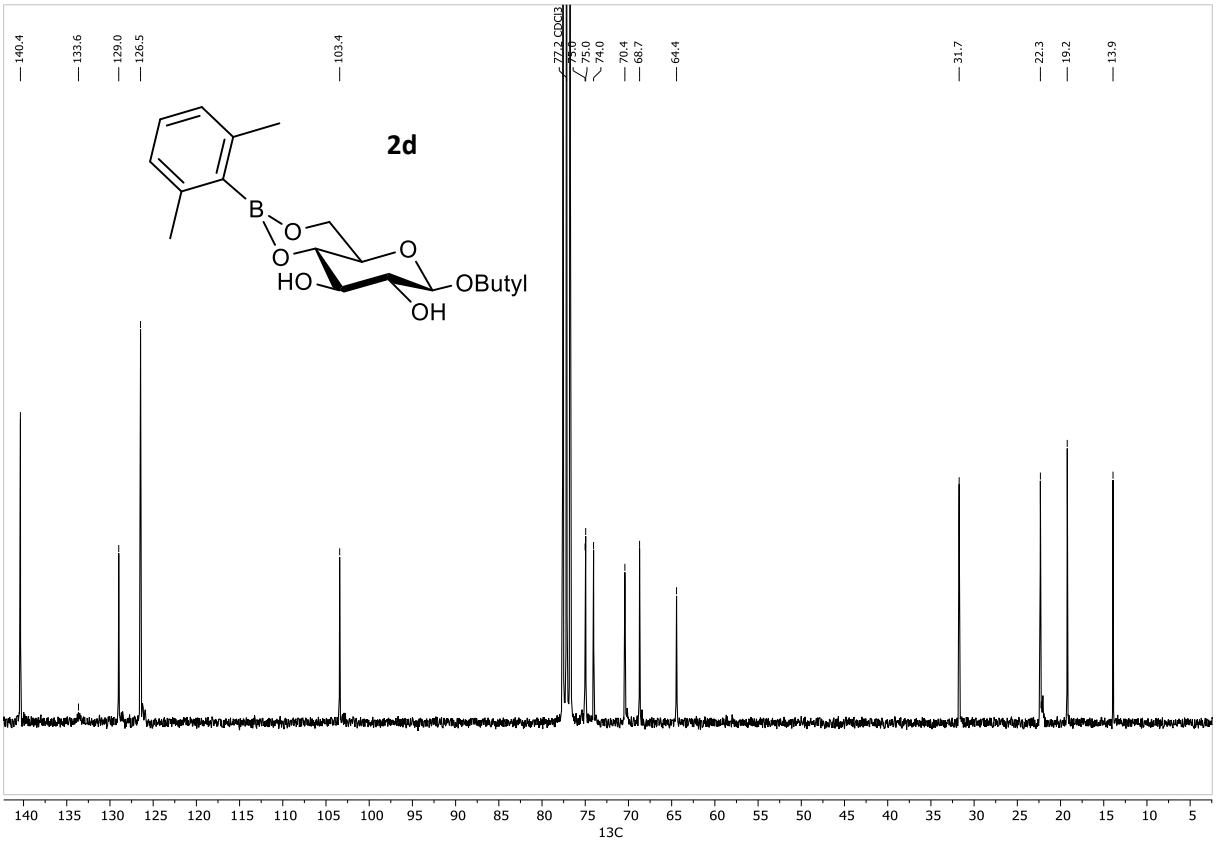

^{13}C NMR spectrum ($CDCl_3$, 75 MHz) of compound **2d**

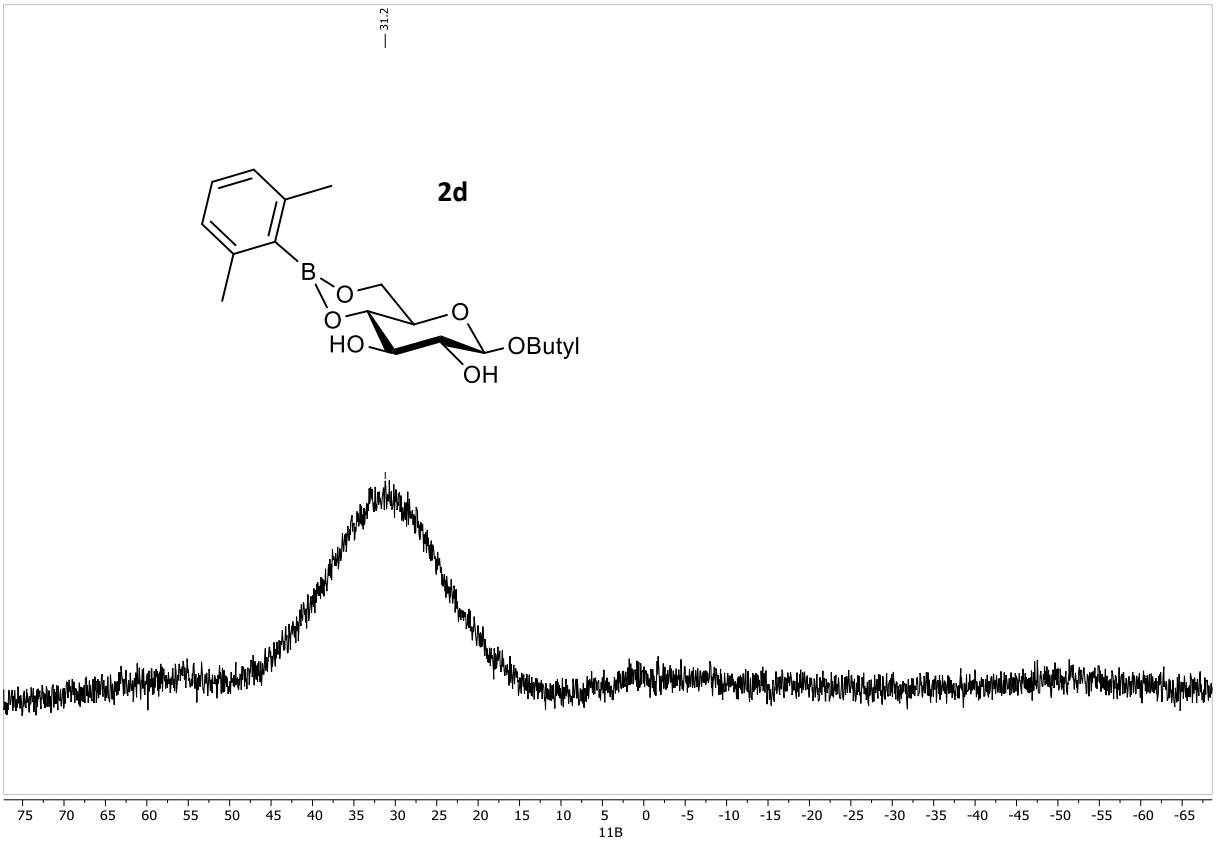

$^{11}B\{1H\}$ NMR ($CDCl_3$, 96 MHz) of compound **2d**

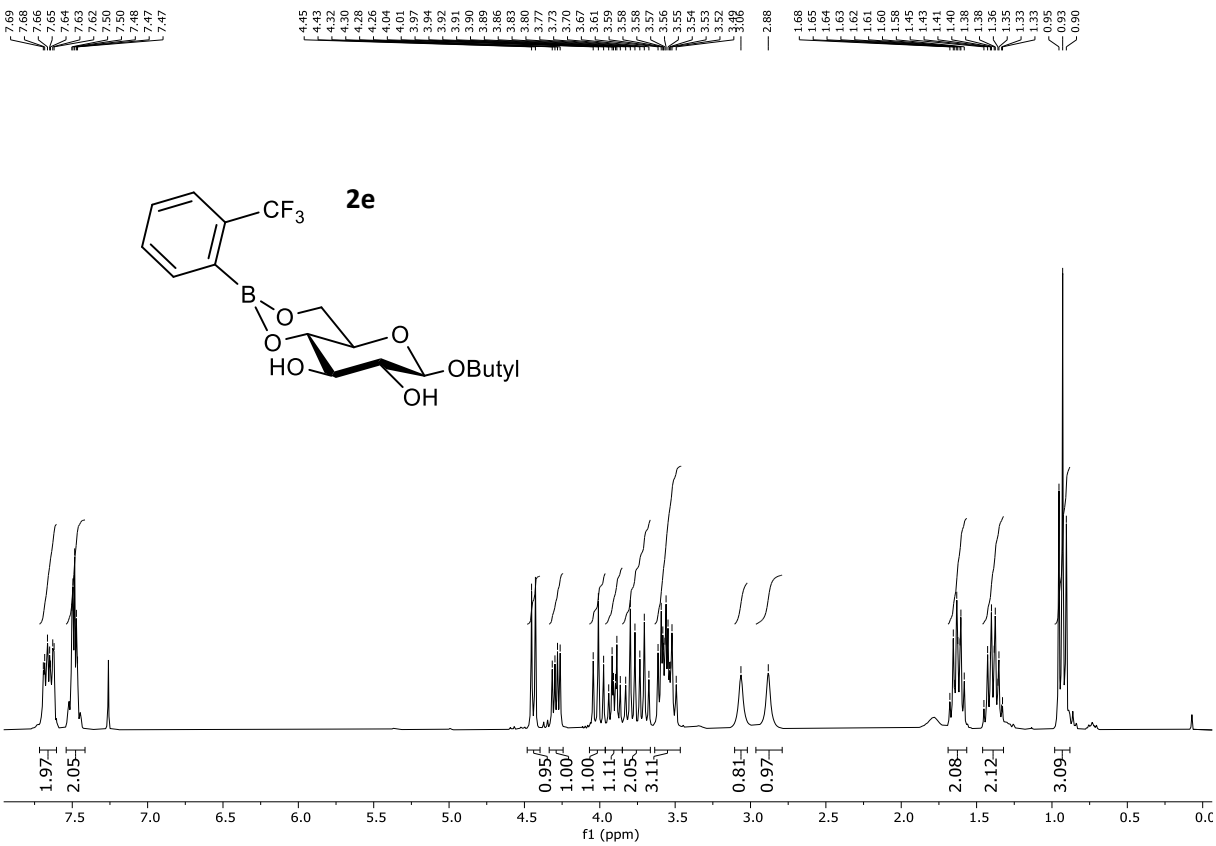

^{1}H NMR spectrum ($CDCl_3$, 300 MHz) of compound **2e**

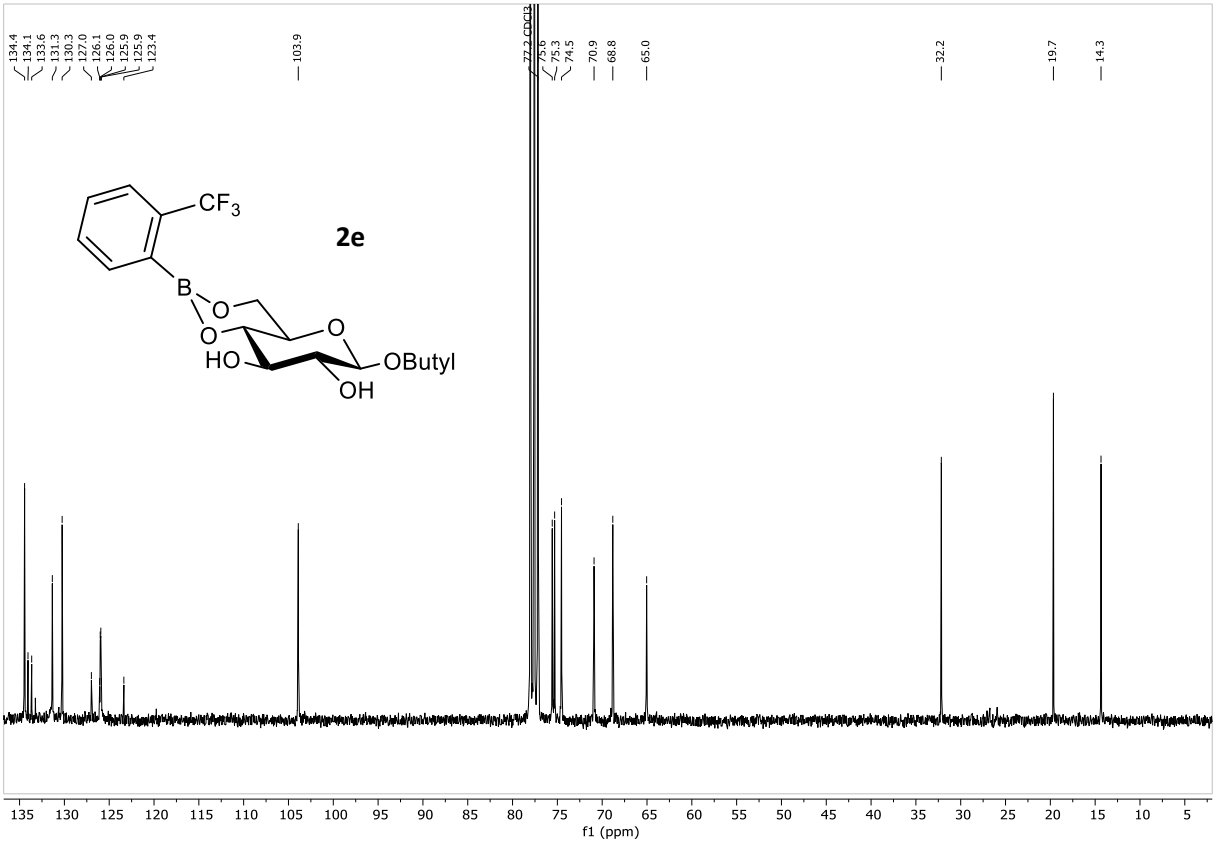

^{13}C NMR spectrum ($CDCl_3$, 75 MHz) of compound **2e**

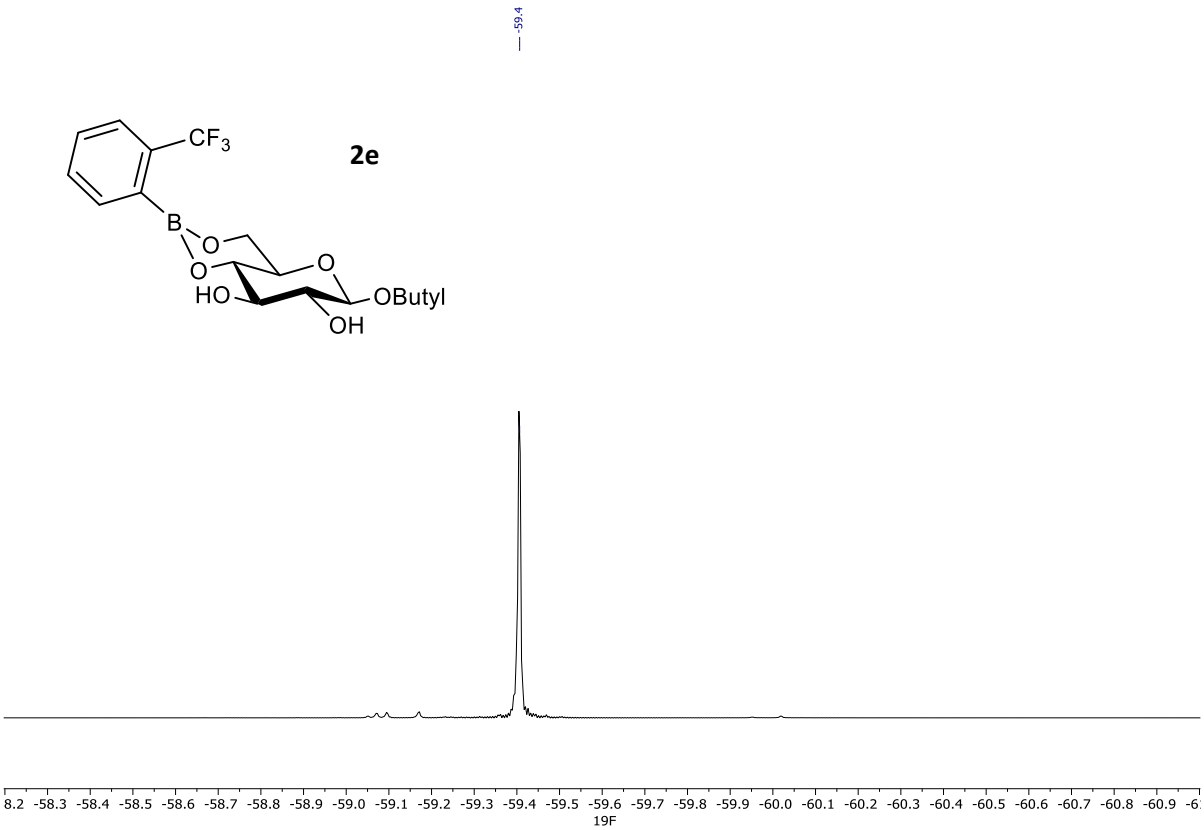

$^{19}F\{1H\}$ NMR ($CDCl_3$, 282 MHz) of compound **2e**

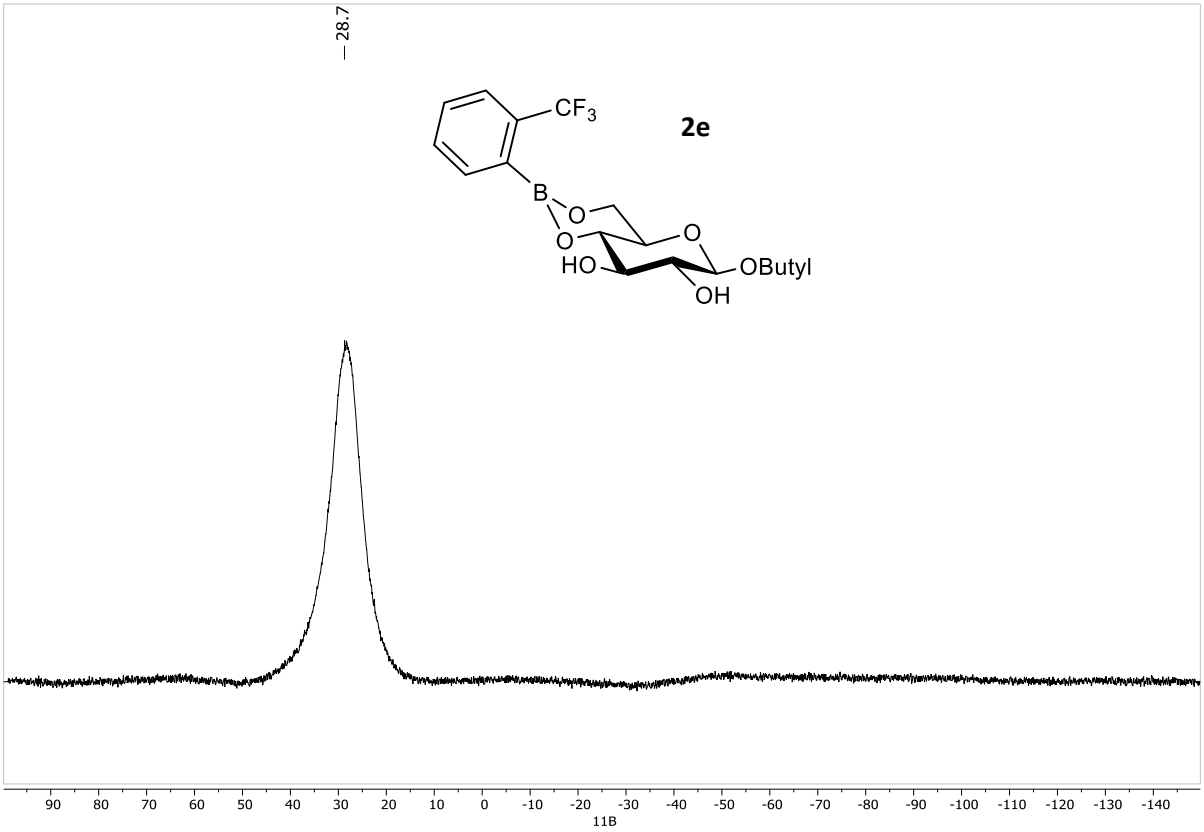

$^{11}B\{1H\}$ NMR ($CDCl_3$, 96 MHz) of compound **2e**

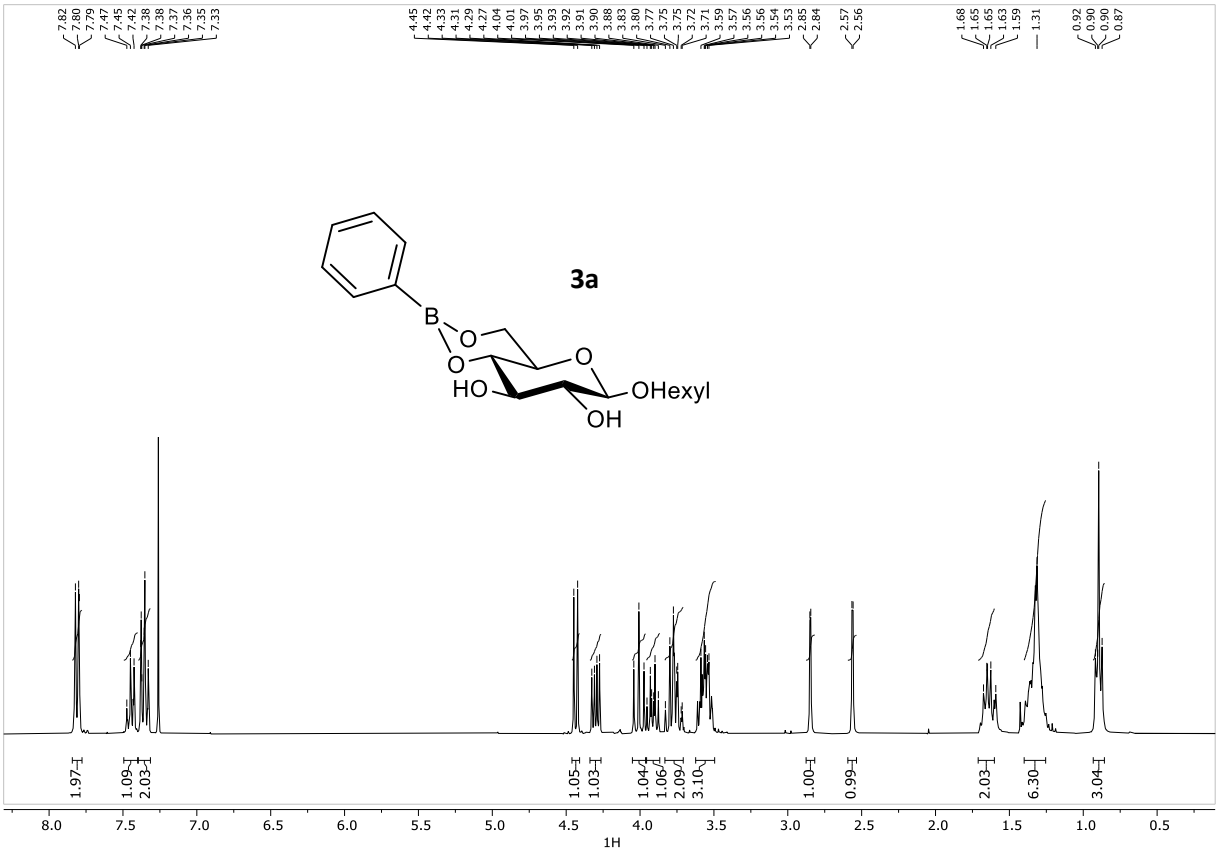

^{1}H NMR spectrum ($CDCl_3$, 300 MHz) of compound **3a**

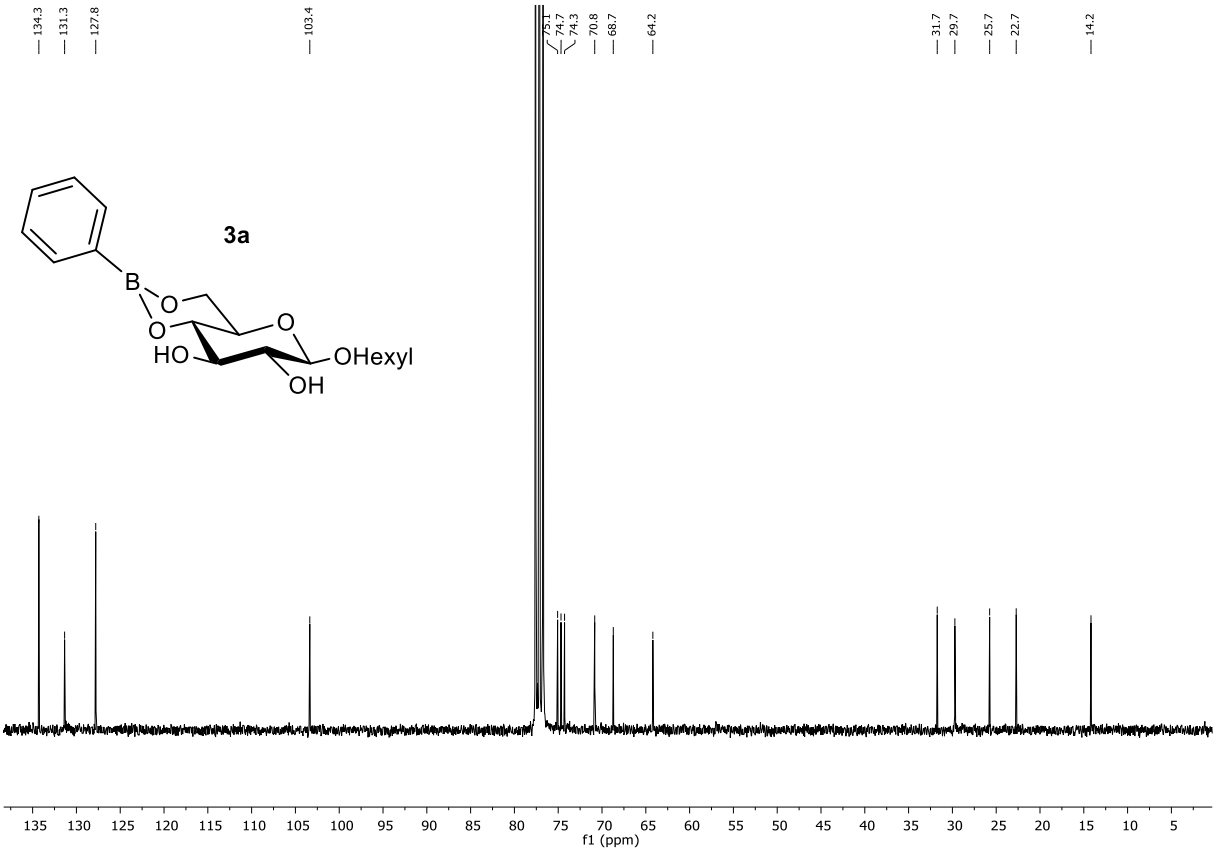

^{13}C NMR spectrum ($CDCl_3$, 75 MHz) of compound **3a**

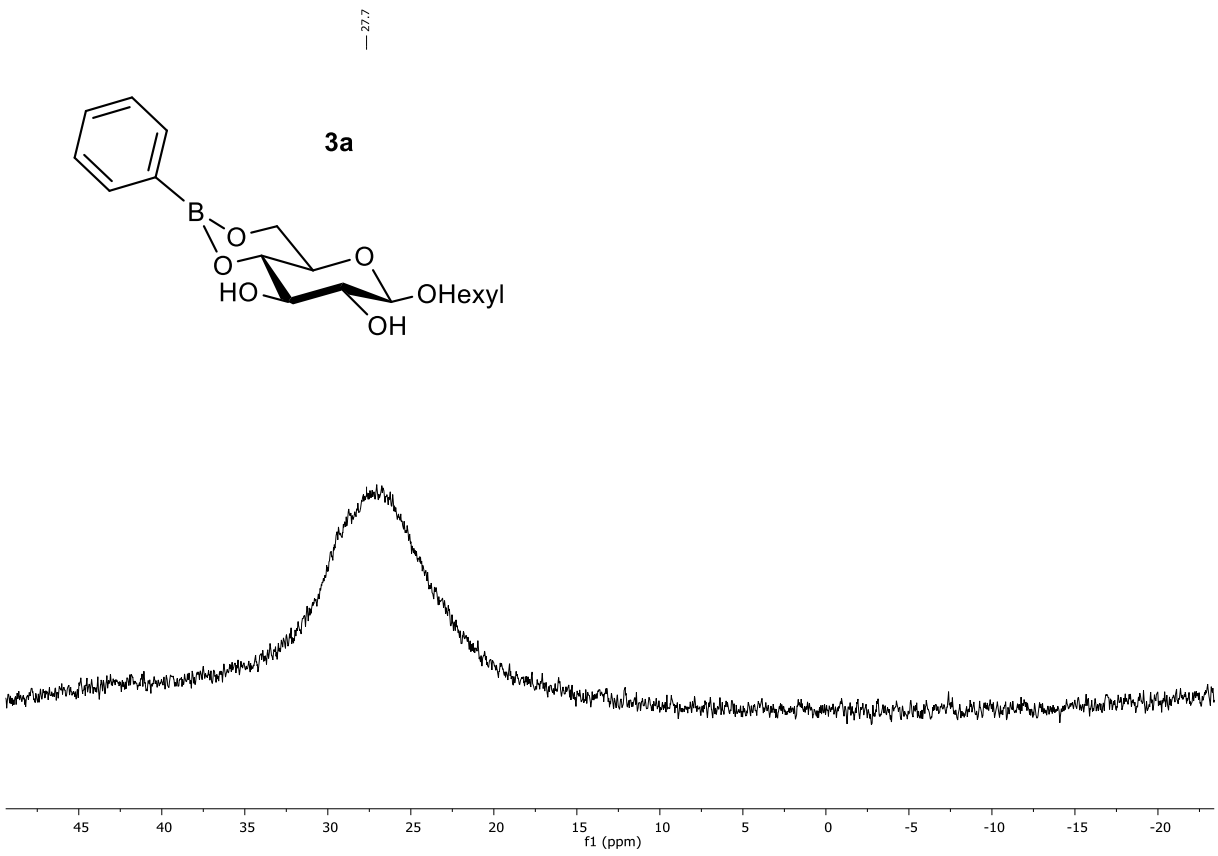

$^{11}B\{1H\}$ NMR ($CDCl_3$, 96 MHz) of compound **3a**

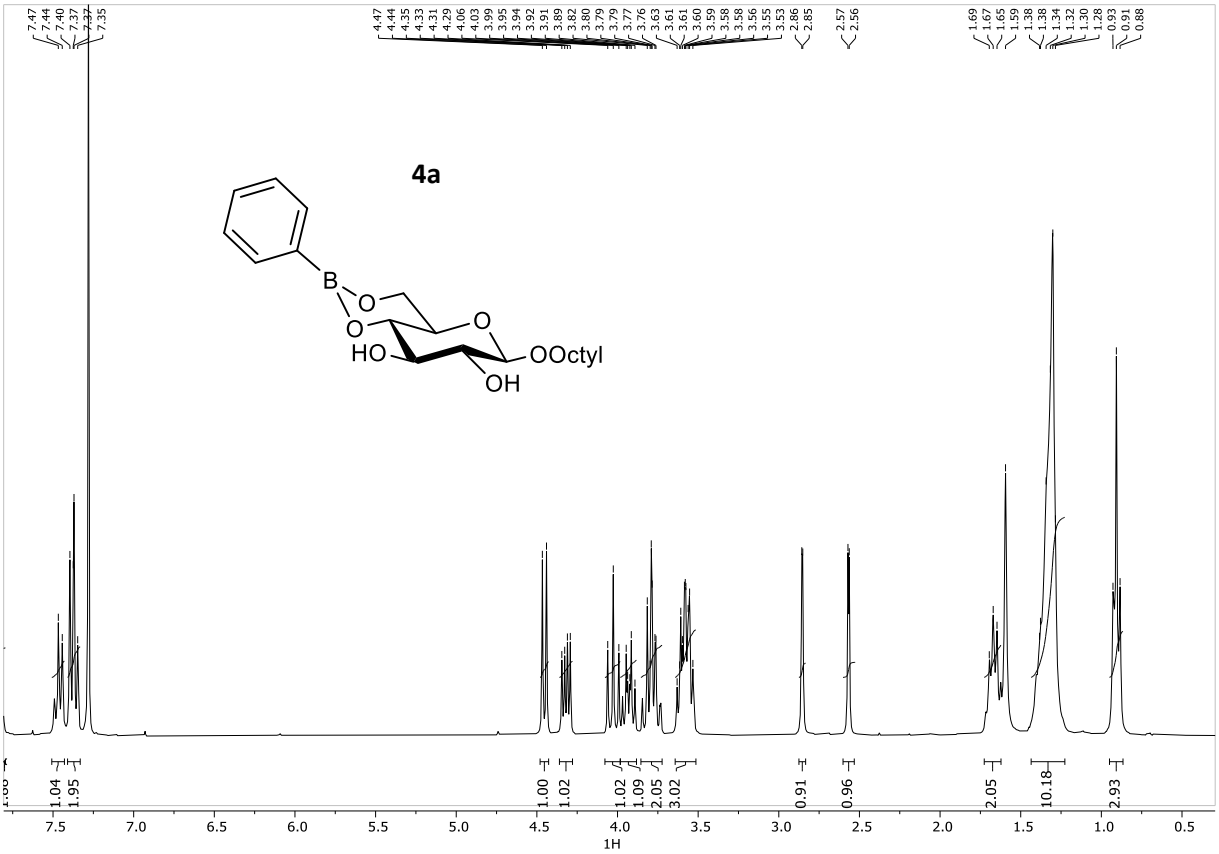

^{1}H NMR spectrum ($CDCl_3$, 300 MHz) of compound **4a**

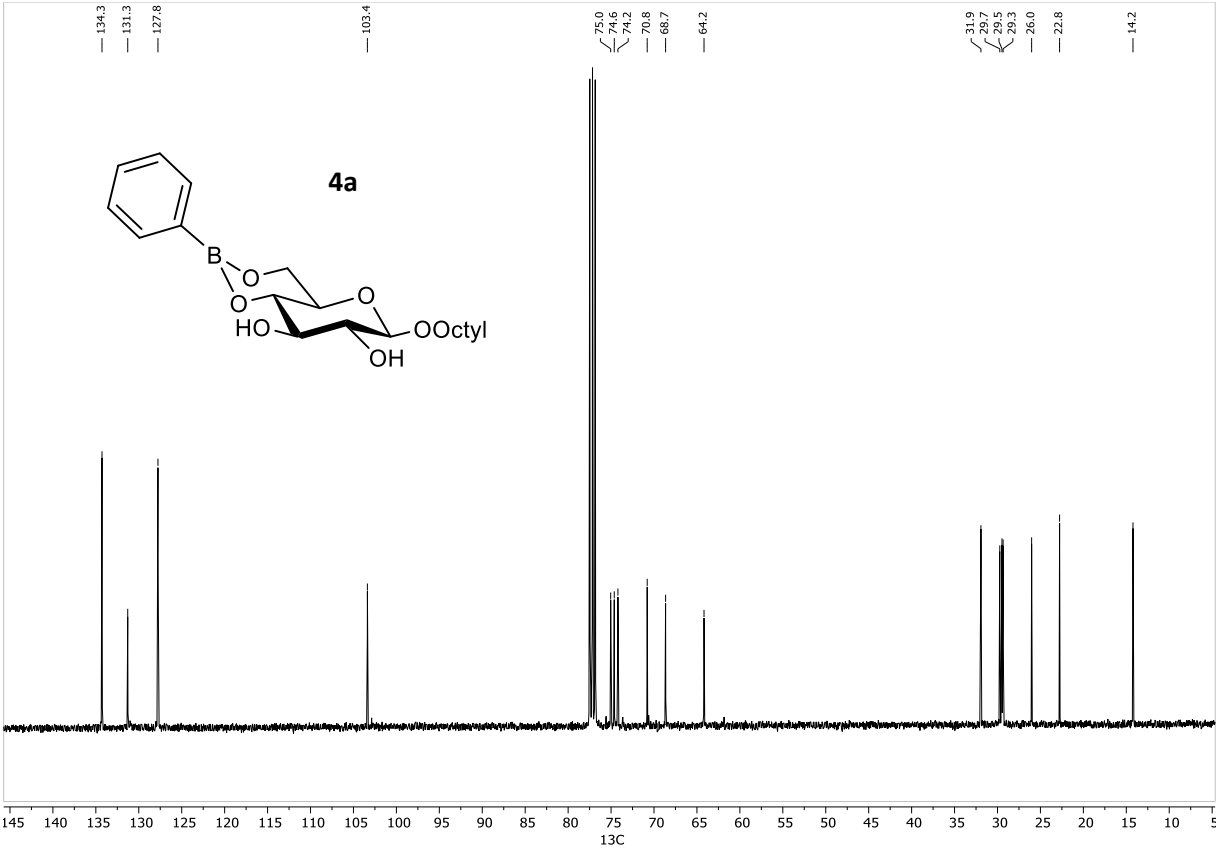

^{13}C NMR spectrum ($CDCl_3$, 75 MHz) of compound **4a**

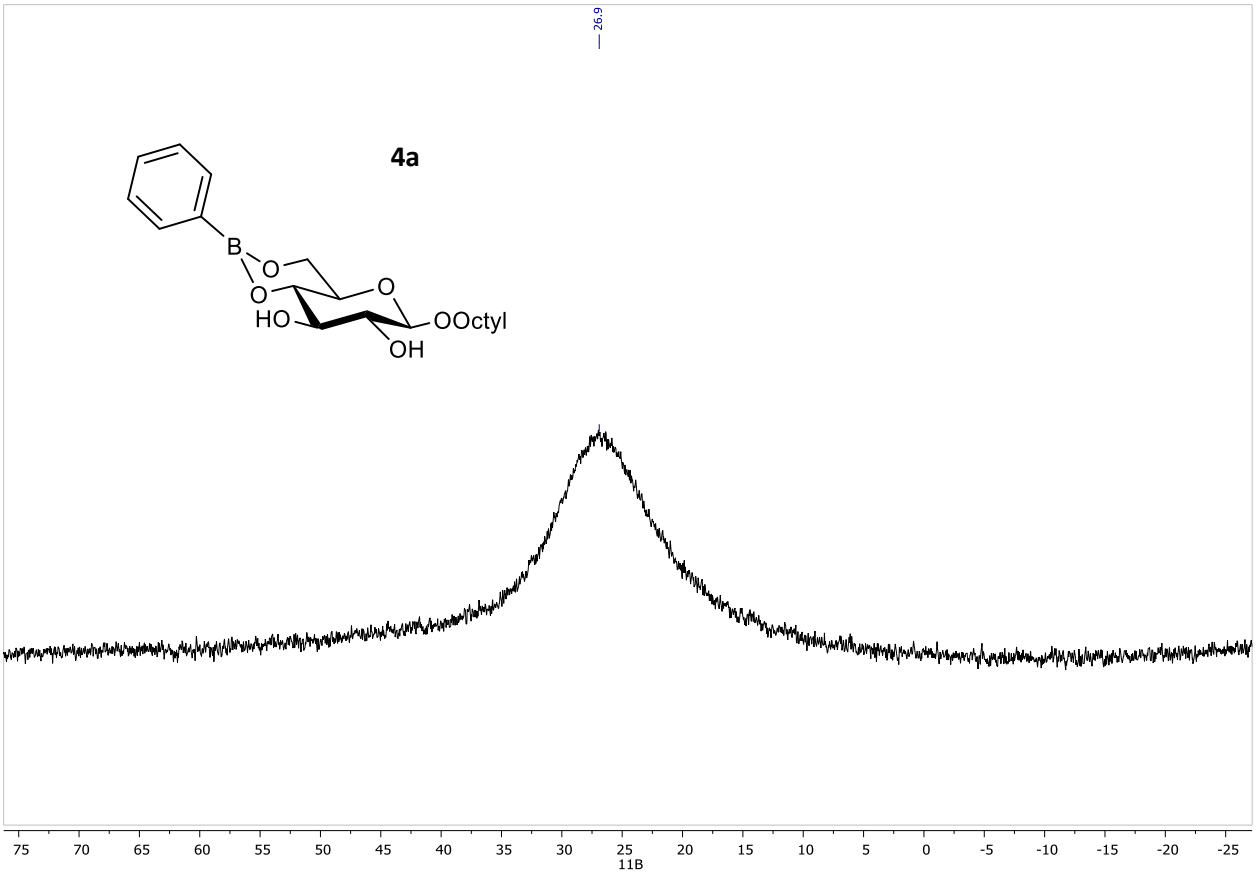

$^{11}B\{1H\}$ NMR ($CDCl_3$, 96 MHz) of compound **4a**

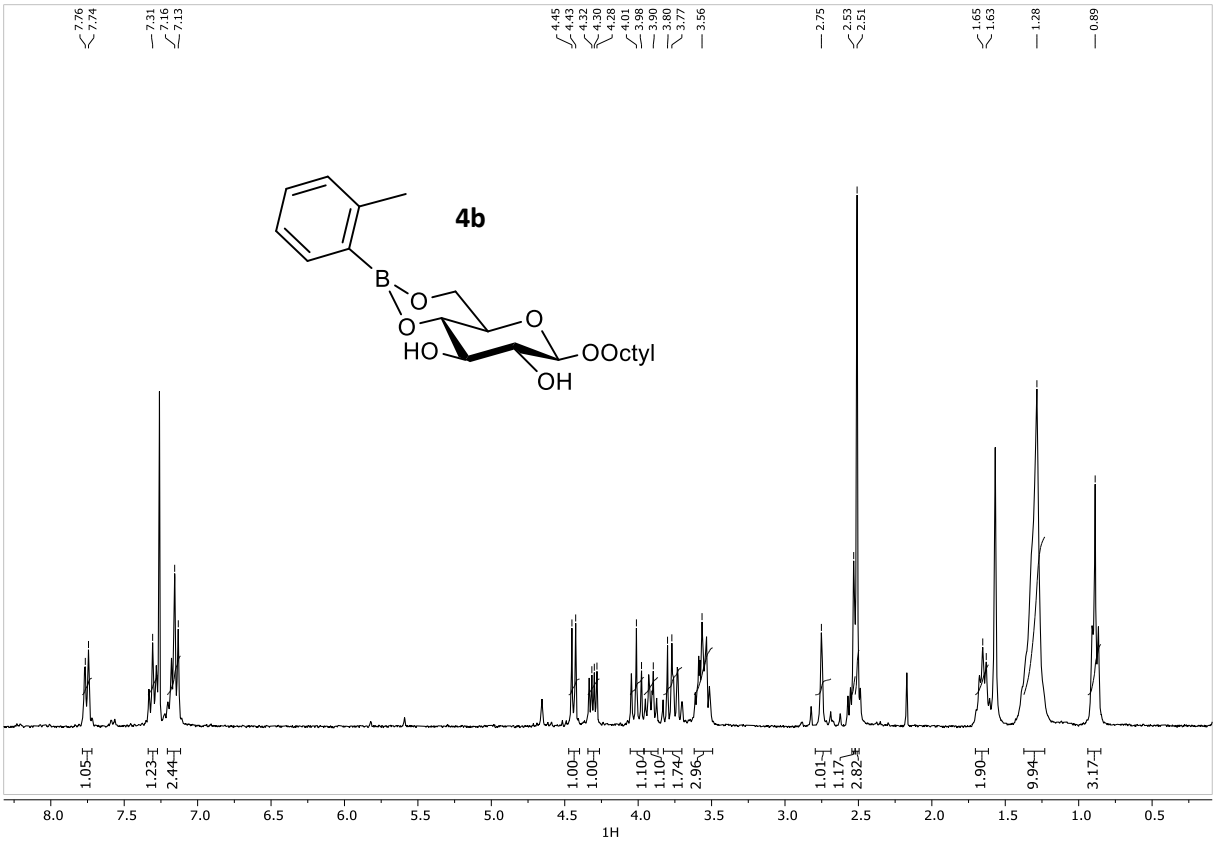

^{1}H NMR spectrum ($CDCl_3$, 300 MHz) of compound **4b**

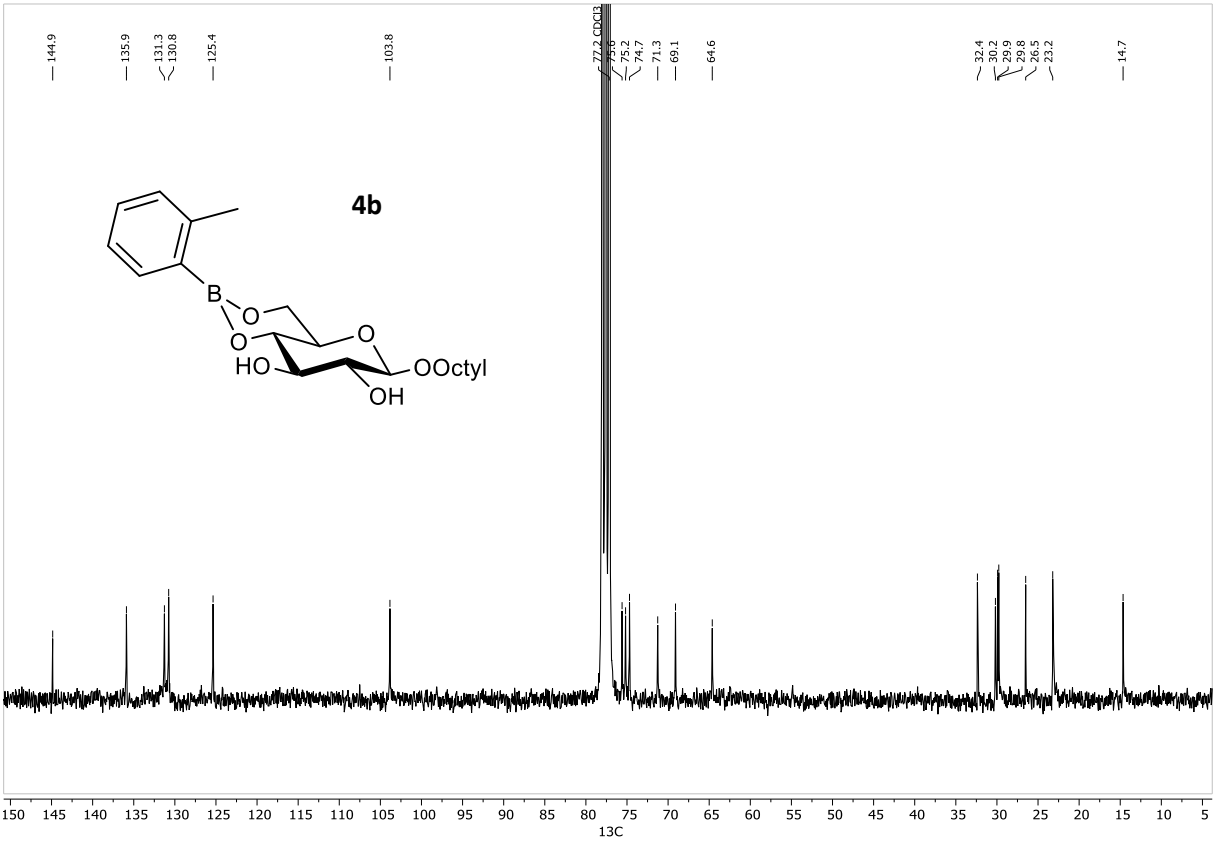

^{13}C NMR spectrum ($CDCl_3$, 75 MHz) of compound **4b**

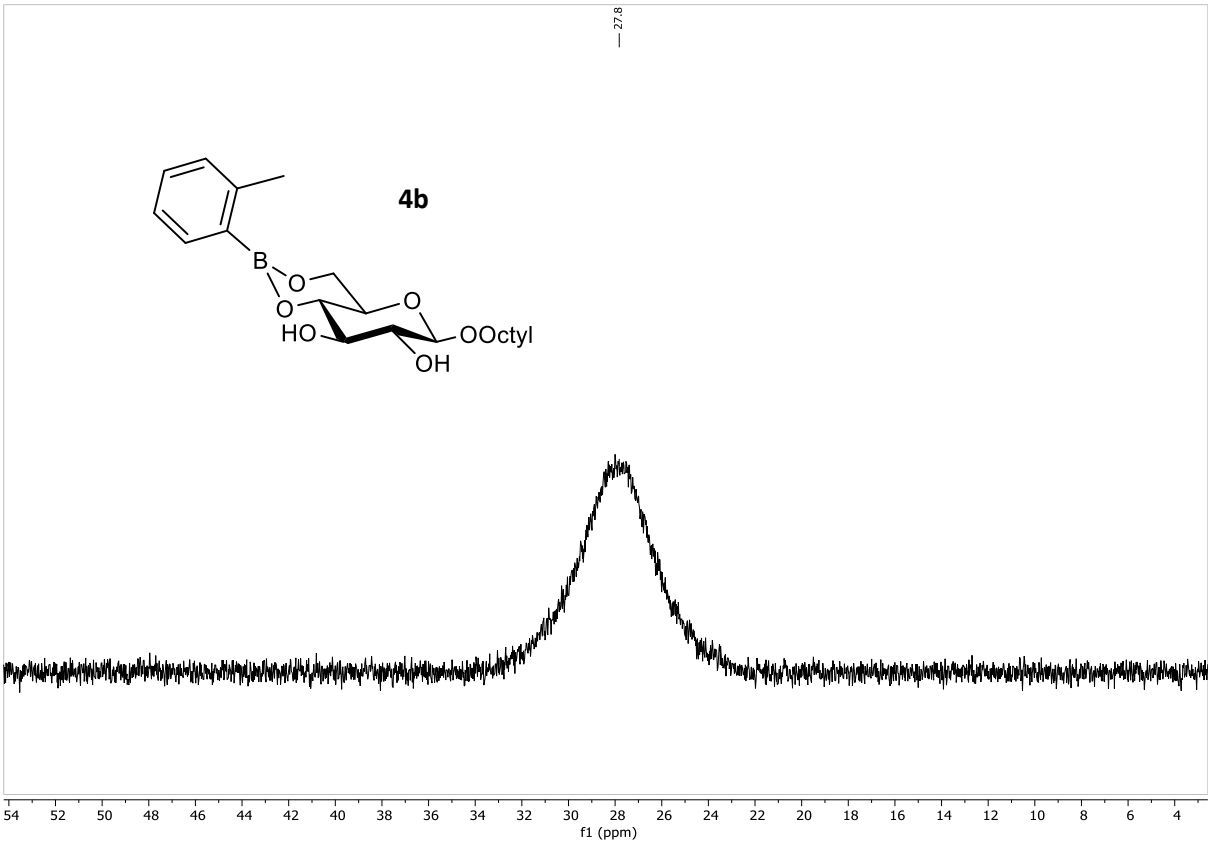

$^{11}B\{1H\}$ NMR ($CDCl_3$, 96 MHz) of compound **4b**

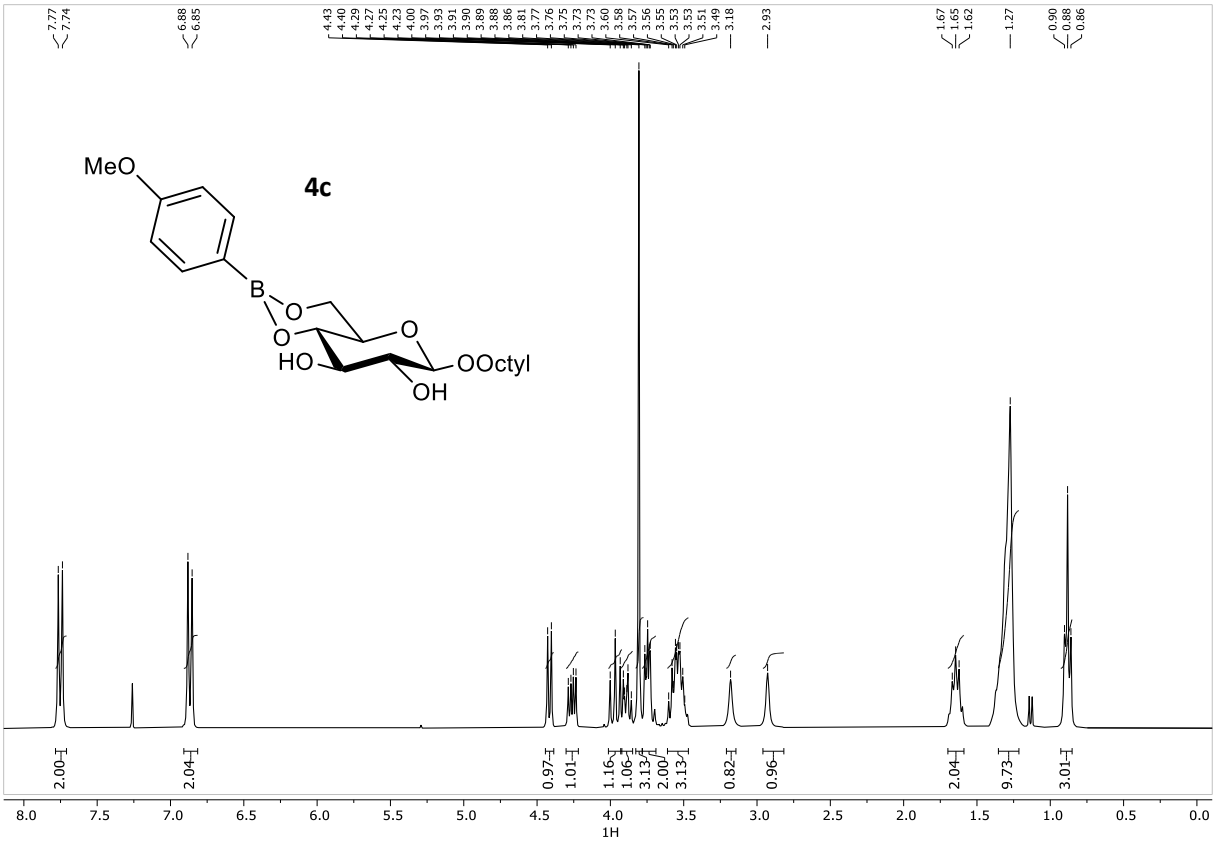

^{1}H NMR spectrum ($CDCl_3$, 300 MHz) of compound **4c**

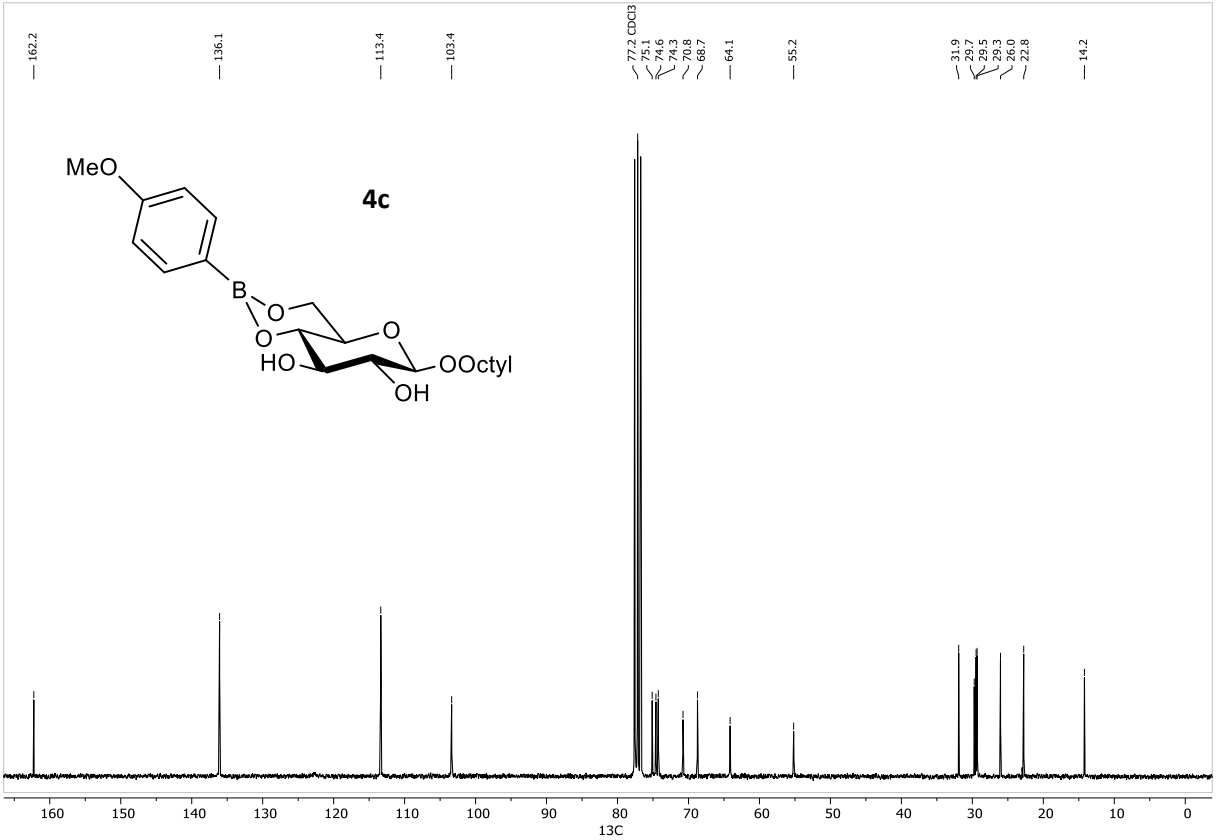

^{13}C NMR spectrum ($CDCl_3$, 75 MHz) of compound **4c**

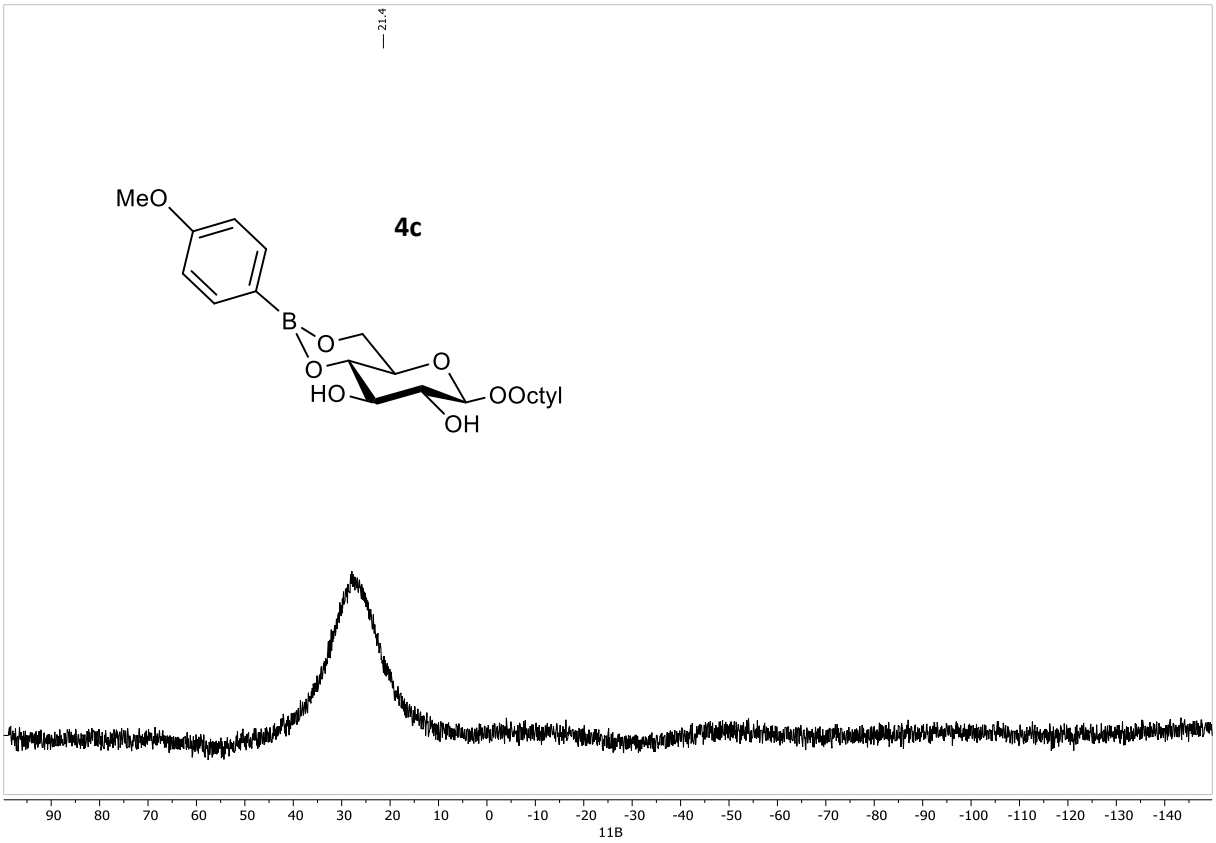

$^{11}B\{1H\}$ NMR ($CDCl_3$, 96 MHz) of compound **4c**

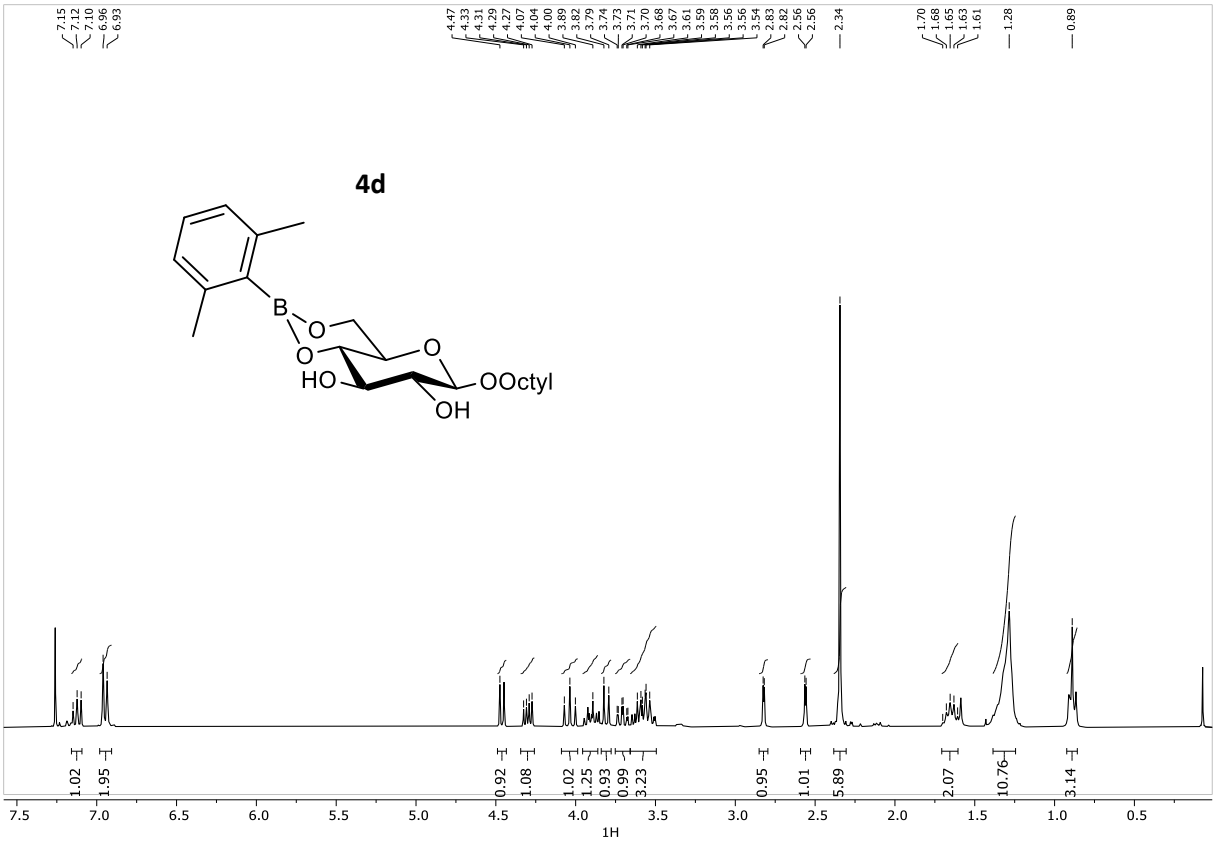

^{1}H NMR spectrum ($CDCl_3$, 300 MHz) of compound **4d**

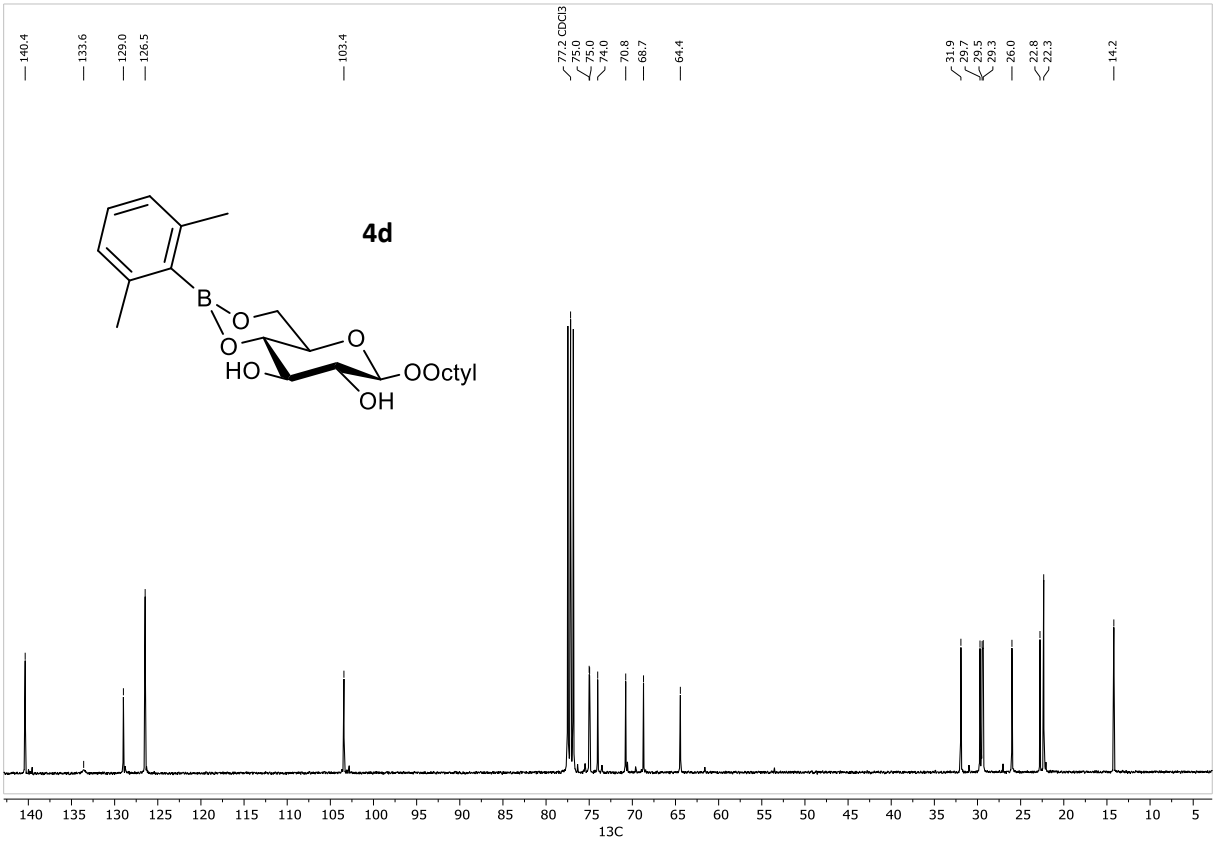

^{13}C NMR spectrum ($CDCl_3$, 101 MHz) of compound **4d**

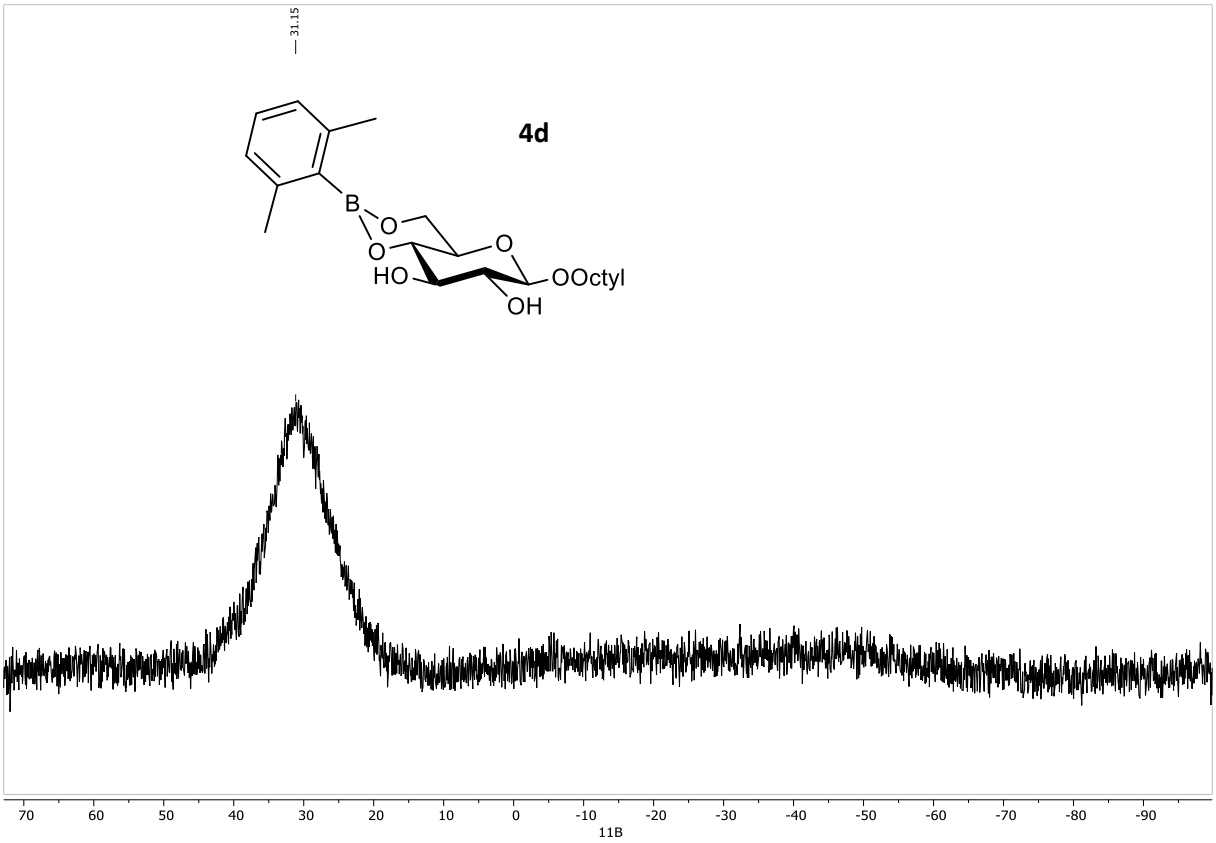

$^{11}B\{1H\}$ NMR ($CDCl_3$, 96 MHz) of compound **4d**

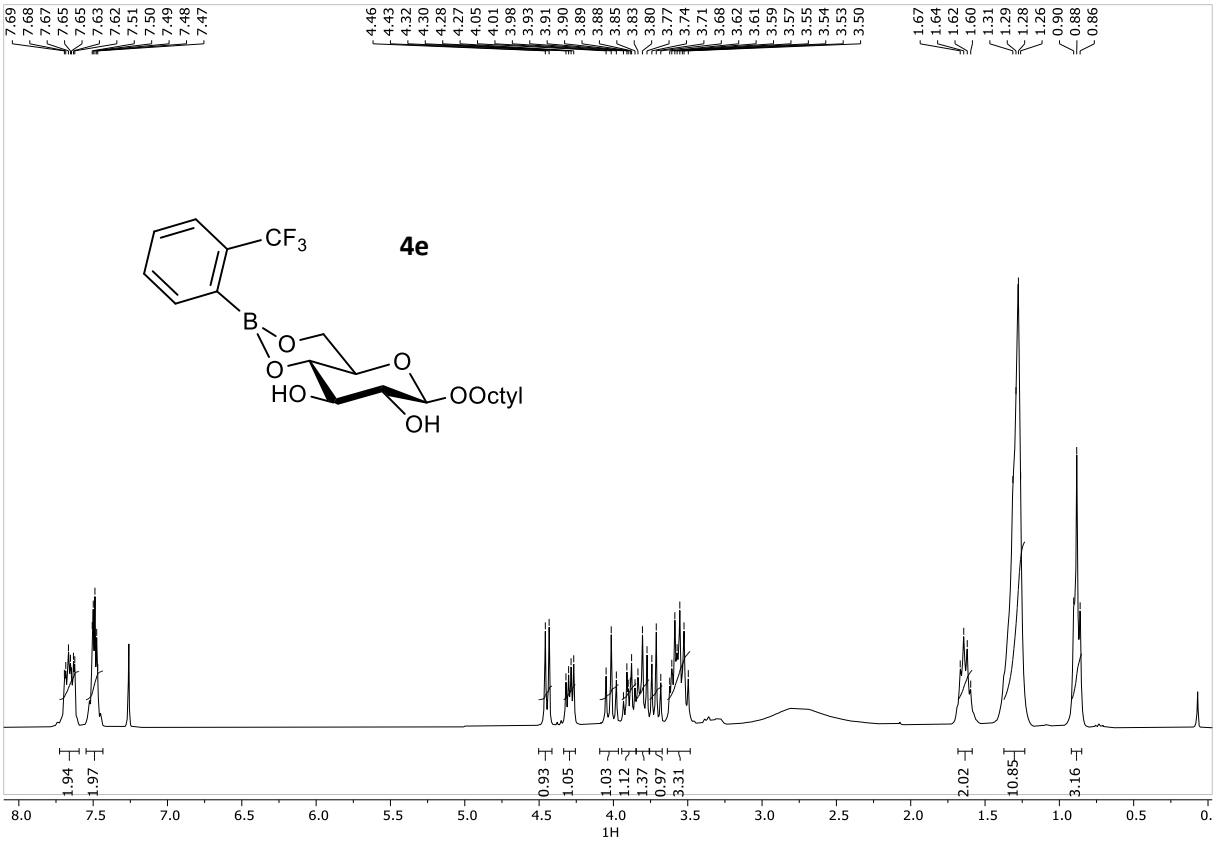

^{1}H NMR spectrum ($CDCl_3$, 300 MHz) of compound **4e**

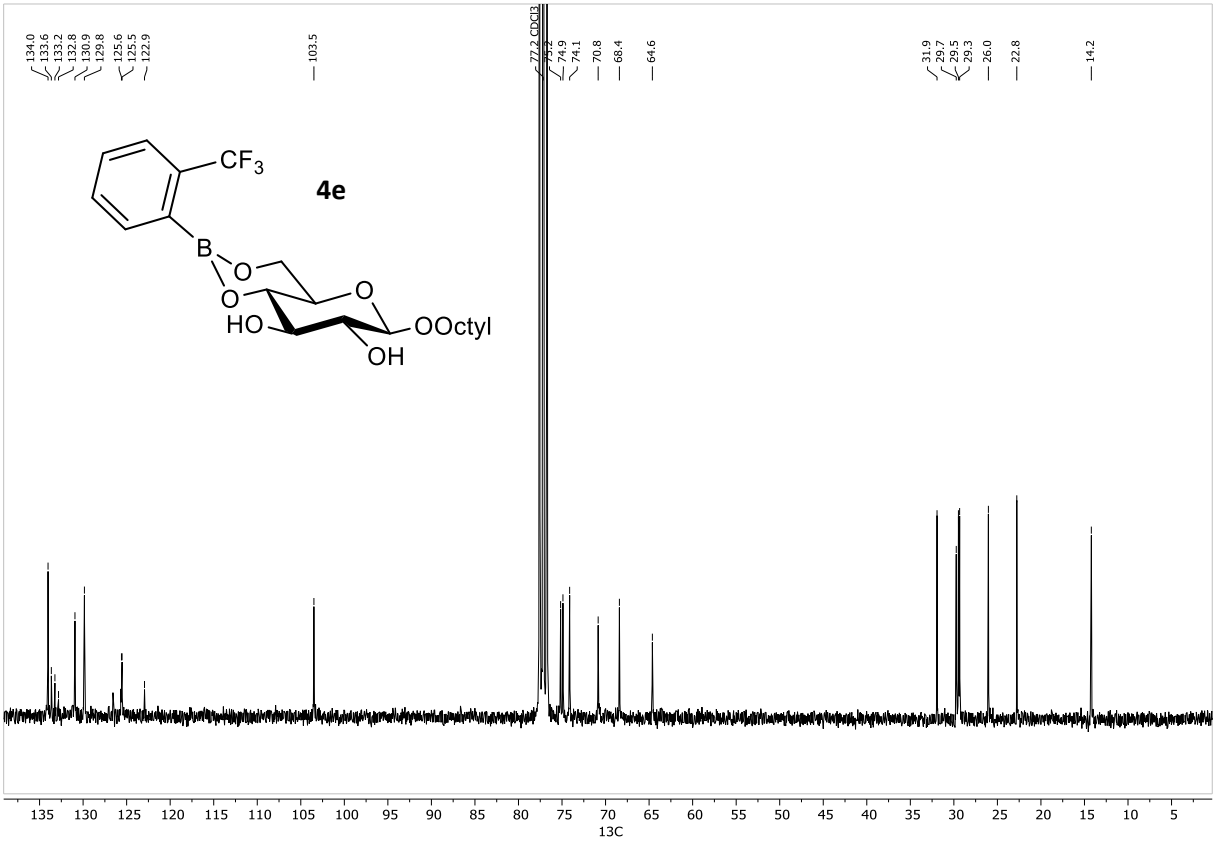

^{13}C NMR spectrum ($CDCl_3$, 75 MHz) of compound **4e**

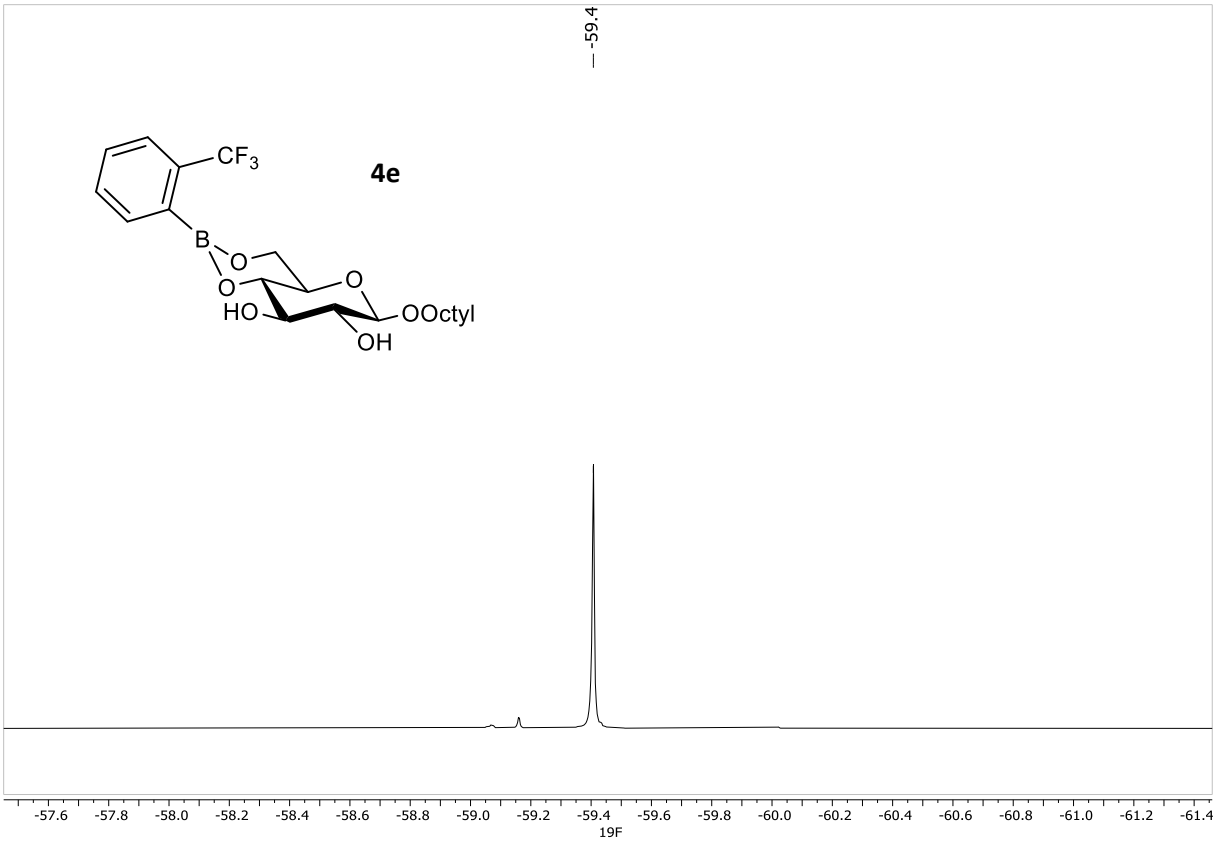

$^{19}F\{1H\}$ NMR ($CDCl_3$, 282 MHz) of compound **4e**

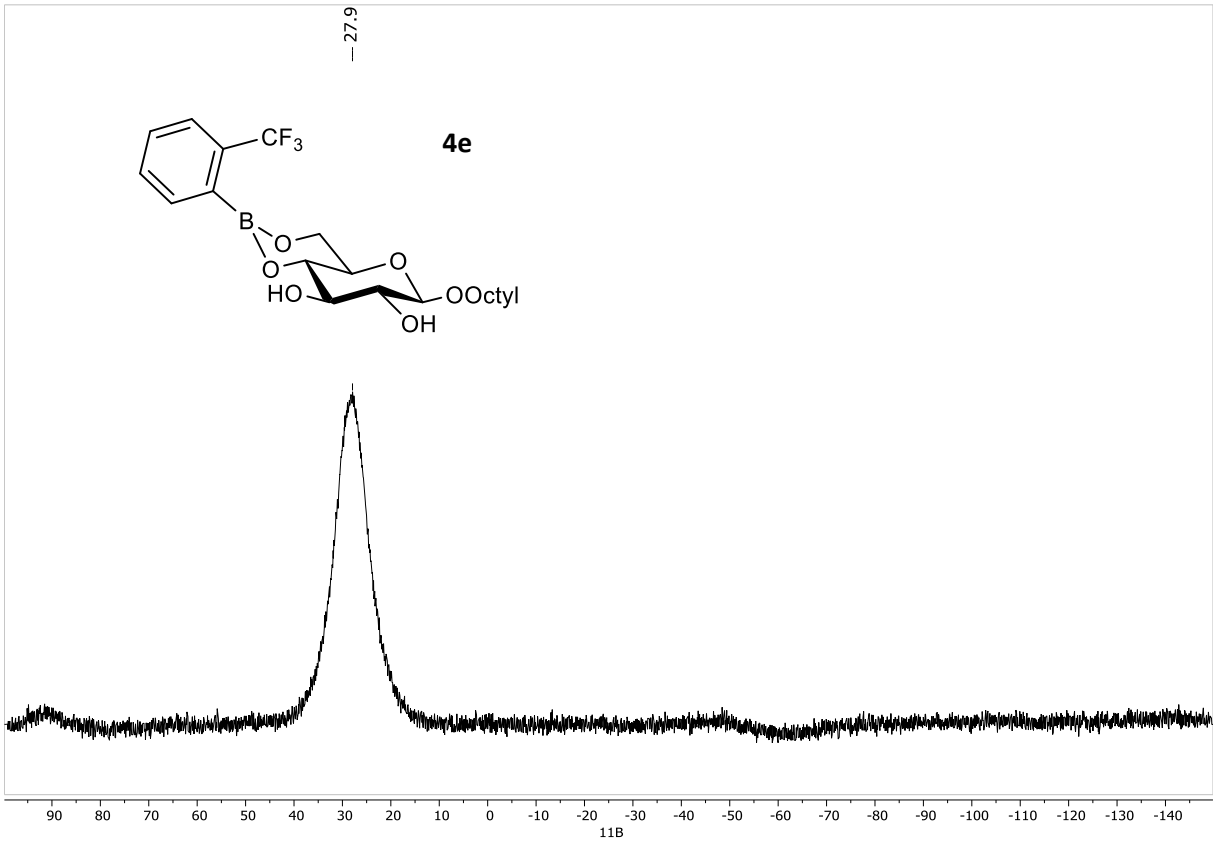

$^{11}B\{1H\}$ NMR ($CDCl_3$, 96 MHz) of compound **4e**

S2. Rheometry of gels in cyclohexane and ethyl myristate

Frequency dependent experiment with gel in toluene with **4a** at a strain of 5%.

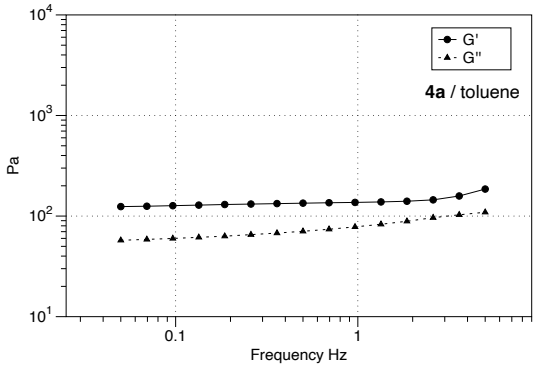

2a cyclohexane

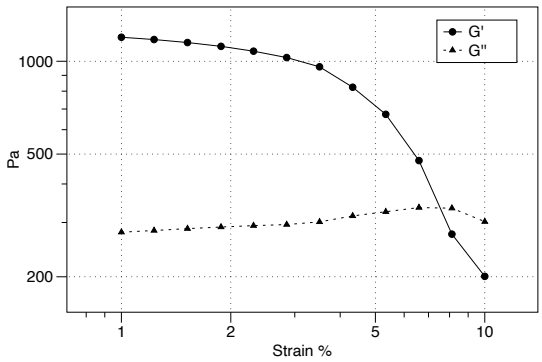

1a Ethyl Myristate

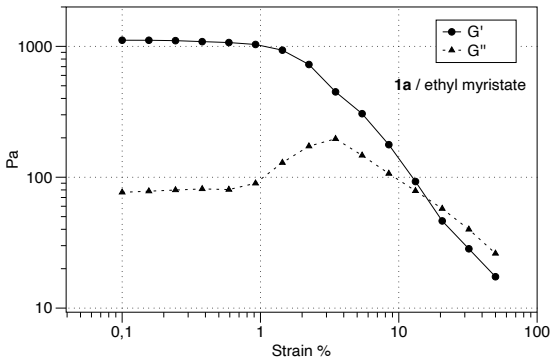

4b Cyclohexane

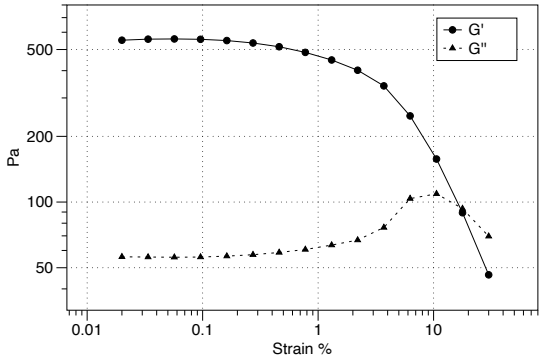

2a Ethyl Myristate

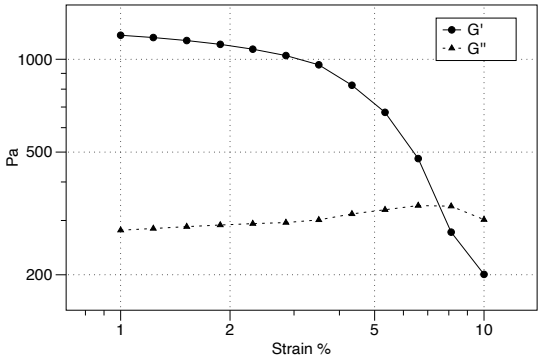

3a Ethyl Myristate

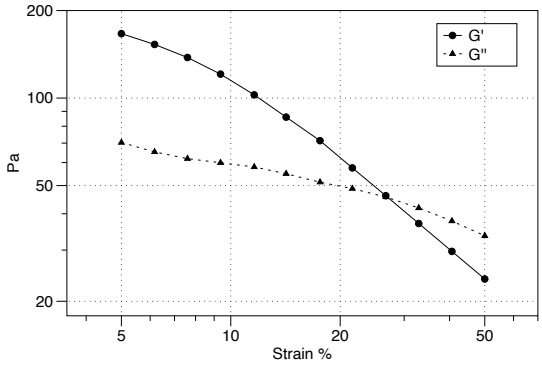

4b Ethyl Myristate

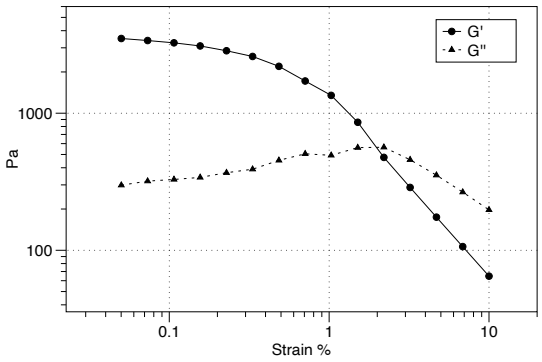

2b Ethyl Myristate

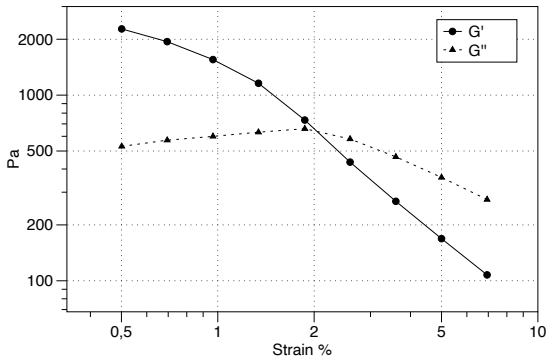

2c Ethyl Myristate

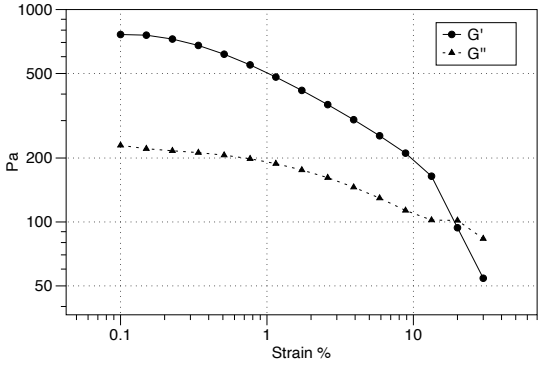

4a Ethyl Myristate

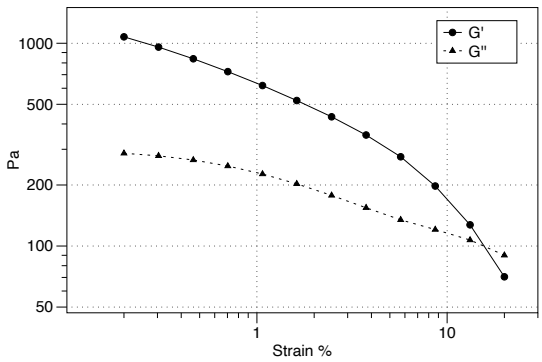

4c Ethyl Myristate

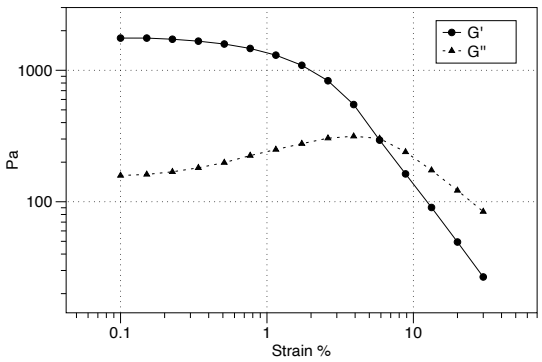

S3. SEM images of xerogel samples (x10 000), bar = 1 μm

All xerogels were obtained from freeze-drying of toluene-based gels.

1a

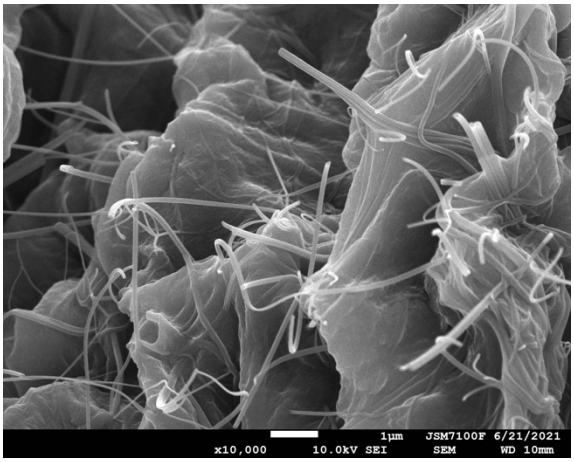

2a (x5000, bar = 5 μm)

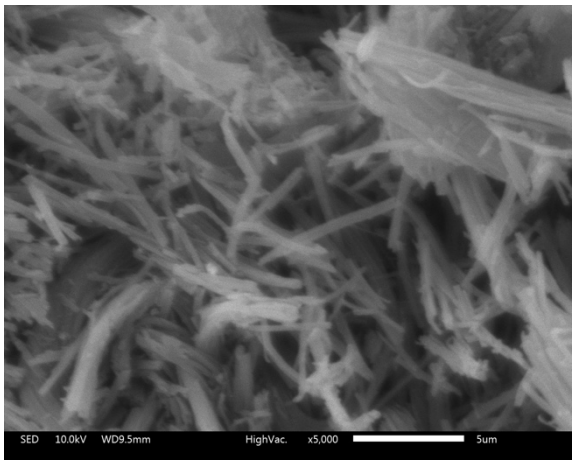

3a

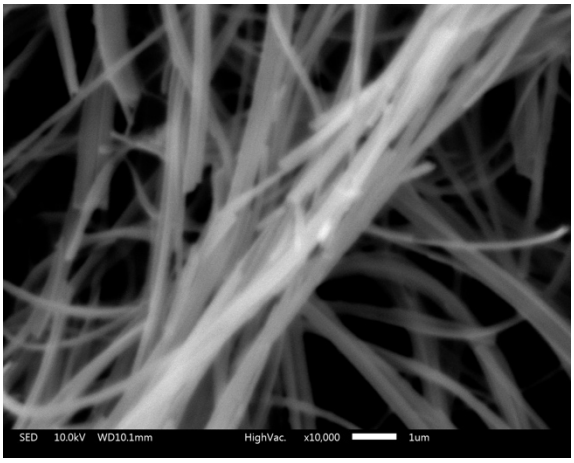

4a

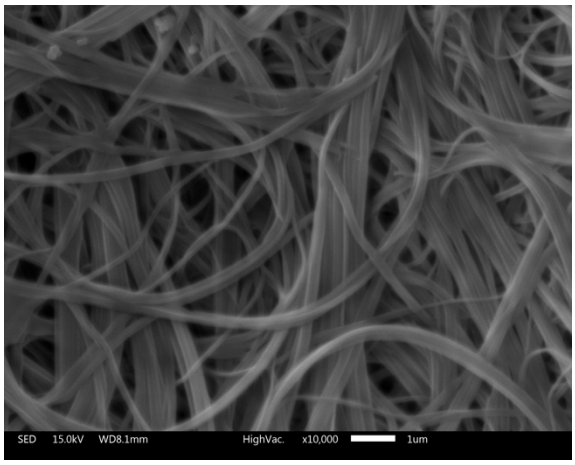

2b

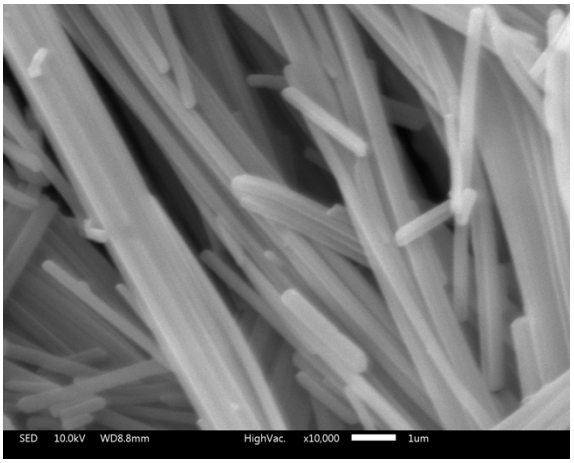

4b

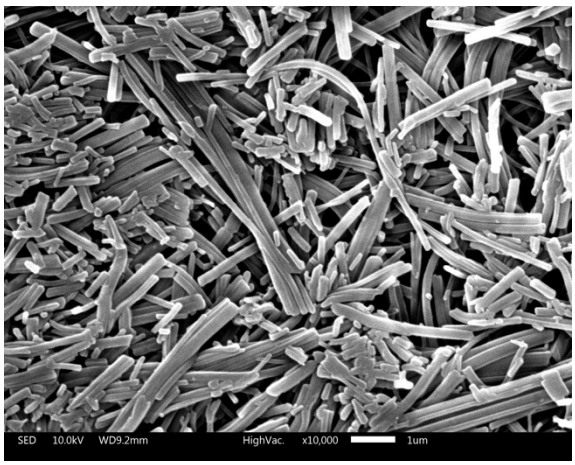

2c

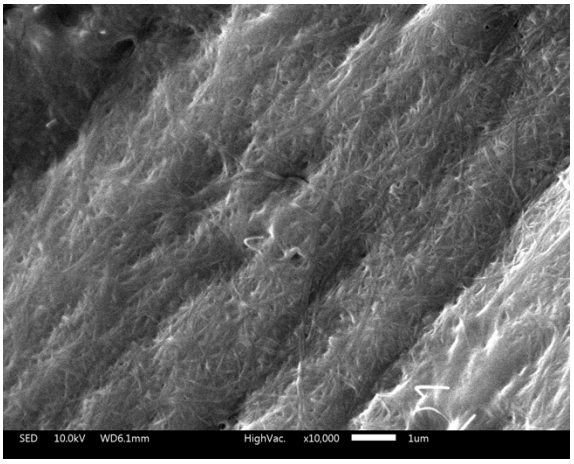
SED 10.0kV WD6.1mm HighVac. x10,000 1um

4c

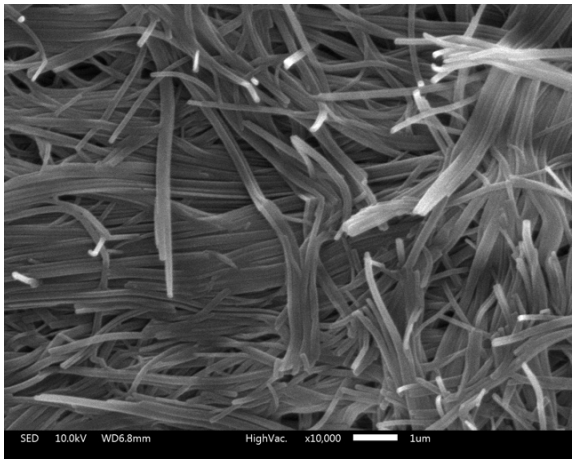
SED 10.0kV WD6.8mm HighVac. x10,000 1um

S4. SAXS Analysis

SAXS analysis (Xerogel of toluene and cyclohexane-based gels with 4b)

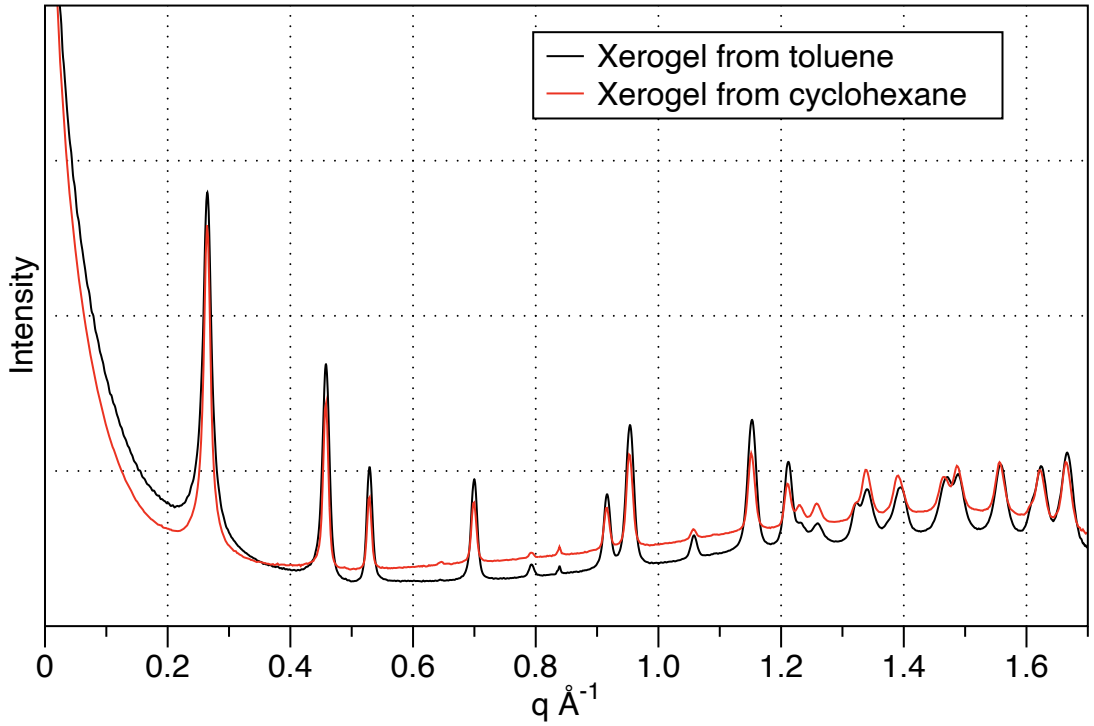

SAXS analysis (Xerogel of toluene-based gel with 3a)

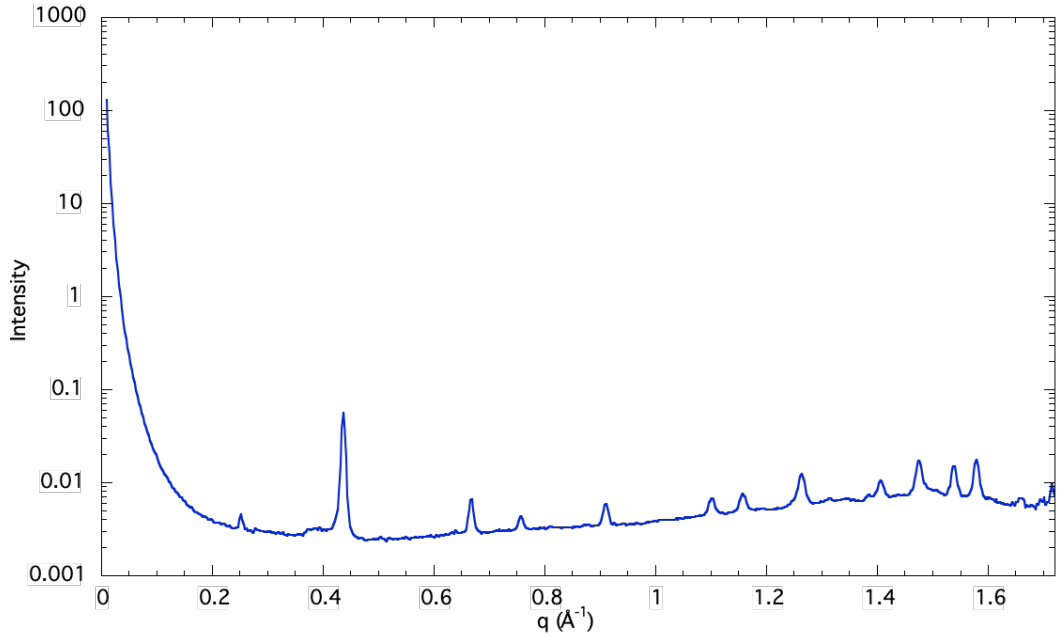

SAXS analysis (Xerogel of toluene-based gel with 3a)

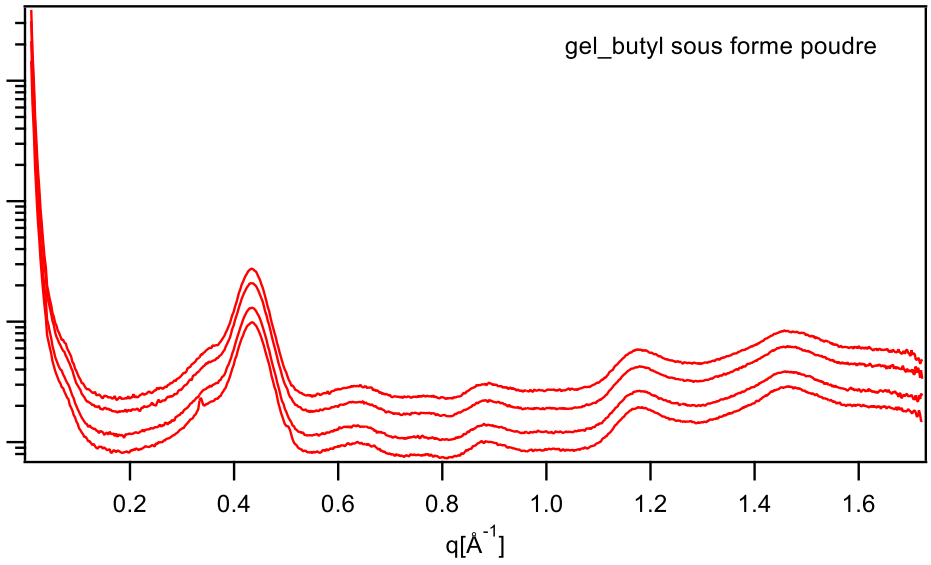

SAXS analysis (Xerogel of toluene-based gel with 4c)

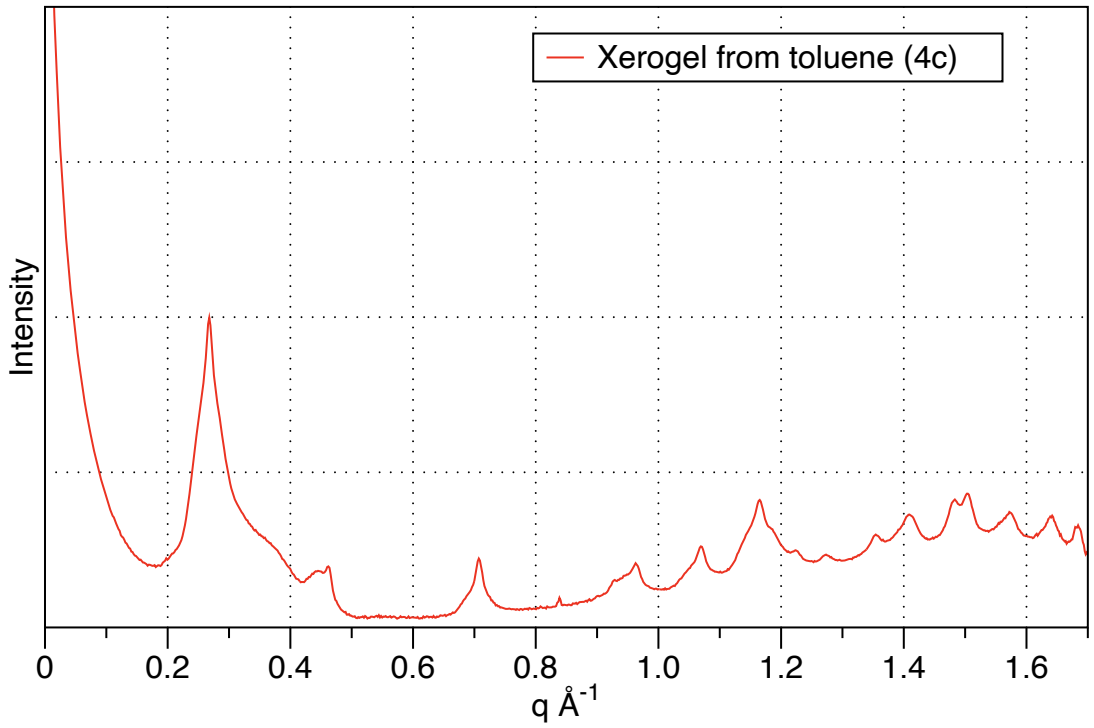

S5. Hydrolysis experiments

Example of water-sensitivity experiments (Organogelator **2a** in toluene 12 mg mL^{-1}). Immersed in water. See butyl2a.gif file for full experiment.

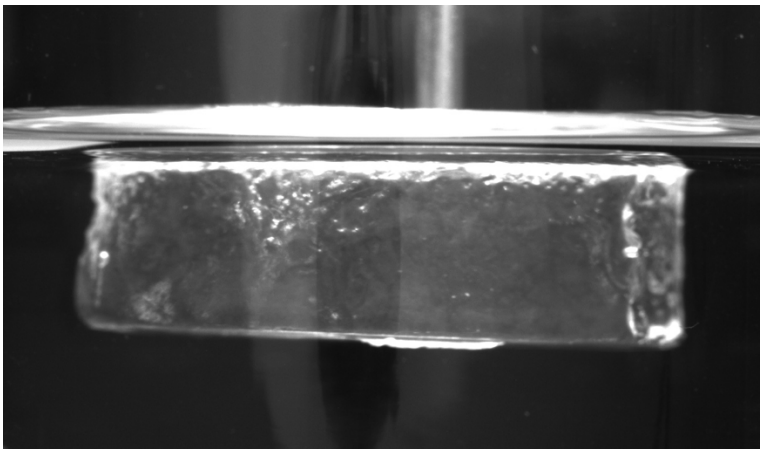

Example of water-sensitivity experiments (Organogelator **2b** in toluene 16 mg mL^{-1}). Immersed in water. See oMebutyl2b.gif file for full experiment.

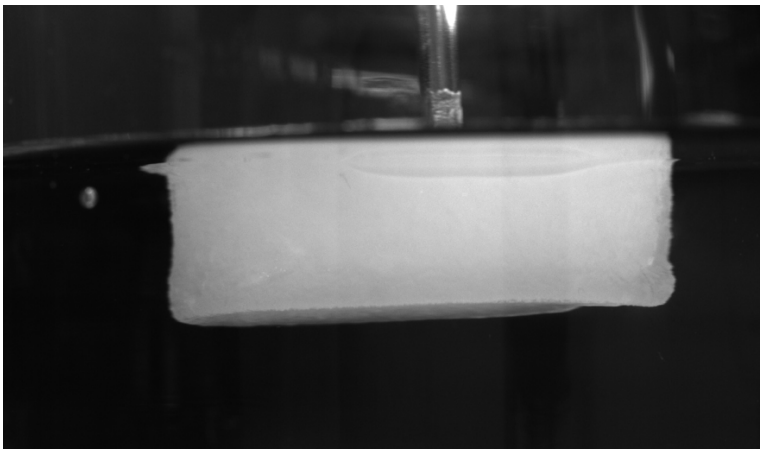

S6. Theoritical and computational part

S6.1 - DFT geometric optimizations and levels of theory.

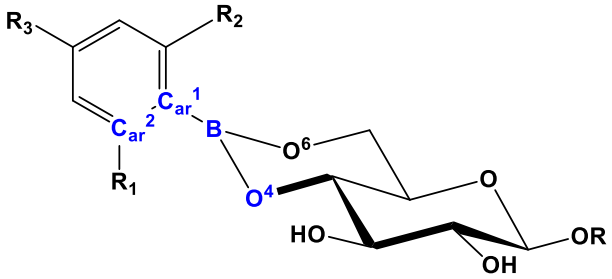

R *aglycone*	*Phenyl ring substituents*			
		R_1	R_2	R_3
R= (n-Pr): **1**,	**a**	H	H	H
(n-Bu): **2**,	**b**	CH_3	H	H
(n-Hex): **3**,	**c**	H	H	OCH_3
(n-Oct): **4**.	**d**	CH_3	CH_3	H
	e	CF_3	H	H

Figure S6.1: Main torsion angle on the arylboronate alkylglucosides according to the aromatic ring (R_1, R_2, R_3) substitution and the alkyl chain aglycones (R) **(α: Car^2-Car^1-B-O^4)**.

Entry	Functional and basis set combinations	Torsion angle α (°)		Distances B…H_3C (Å)		Ref.
		2b	2d	2b	2d	
1	LC-BOP/cc-pVTZ #	--	65.50	--	2.965	[1]
2	B3LYP / 6-311+G(d,p)	1.98	52.11	3.078	2.820	[2-5]
3	B3LYP/cc-pVTZ	1.98	51.3	3.078	2.912	[6-8]
4	M062X/cc-pVTZ	4.76	46.80	3.030	2.890	[9,10]
5	ωB97XD/cc-pVTZ	2.57	54.99	3.066	2.815	[11,12]

Table S6.1: Comparison between different levels of theory to describe conformational modifications of arylboronate of alkylglucosides from chosen parameters. (# used on aryl-1,3,2-dioxaborinane models).

S6.2 – Characteristic geometric parameters of boronate function at ωB97XD/cc-pVTZ level of theory.

Entry	Figure S1 / alkyl chains (R)		1a	2a	3a	4a
A1	Torsion α (°)		2.63	2.58	2.45	2.64
A2	Distance (Å) covalent bonds	B-Car1	1.561	1.561	1.560	1.561
		B-O4	1.369	1.369	1.369	1.369
		B-O6	1.369	1.369	1.369	1.369

Table S6.2.1: Dihedral angles and distances for different alkyl chains at the aglycone position.

Entry	Figure S1 / butyl chain		2a	2b	2c	2d	2e
A1	Torsion α (°)		2.58	2.57	2.68	54.99	52.31
A2	Distance (Å) covalent bonds	B-Car1	1.561	1.566	1.554	1.570	1.574
		B-O4	1.369	1.369	1.371	1.369	1.362
		B-O6	1.369	1.372	1.37&	1.368	1.365
A3	Distance (Å) non-covalent interactions	B..F1	--	--	--	--	2.767
		B..H1	--	3.051	--	2.833	--
		B..H2	--	--		2.801	--

Table S6.2.2: Dihedral angles and distances for different substituents (R1, R2, R3) on the arylboronate butylglucosides.

Entry	Figure S1 / octyl chain		4a	4b	4c	4d	4e
A1	Torsion α (°)		2.64	2.59	2.39	54.47	52.2
A2	Distance (Å) covalent bonds	B-Car1	1.561	1.566	1.554	1.570	1.574
		B-O4	1.369	1.369	1.371	1.369	1.362
		B-O6	1.369	1.372	1.371	1.368	1.365
A3	Distance (Å) non-covalent interactions	B..F1	--	--	--	--	2.837
		B..H1	--	3.044	--	2.834	--
		B..H2	--	--	--	2.811	--

Table S6.2.3: Dihedral angles and distances for different substituents (R1, R2, R3) on the arylboronate octylglucosides.

S6.3 – Molecular orbitals of arylboronates: energy levels and representations.

In order to describe electronic effects, we compared electronic structures for all arylboronates alkylglucosides (compounds: **Cp**) extracting energy levels of molecular orbitals (**MO**, **Tables S6.3.1, S6.3.2, S6.3.3**) and visualizing representations of frontier molecular orbitals (**Figures S6.3.1, S6.3.2, S6.3.3**) as presented here at the selected level of theory ωB97XD/cc-pVTZ.

MO / Cp	1a	2a	3a	4a
LUMO+5	3.2552	3.2509	3.2343	3.1834
LUMO+4	3.0588	3.0522	3.0201	3.0016
LUMO+3	2.8599	2.8525	2.8424	2.8411
LUMO+2	2.8324	2.8280	2.8291	2.8286
LUMO+1	1.9124	1.9137	1.9156	1.9164
LUMO	1.1491	1.1507	1.1529	1.1537
HOMO	-8.7653	-8.7631	-8.7615	-8.7606
HOMO+1	-8.7832	-8.7816	-8.7797	-8.7791
HOMO+2	-9.4943	-9.4894	-9.4845	-9.4831
HOMO+3	-10.0505	-10.0461	-10.0413	-10.0390
HOMO+4	-10.2151	-10.2050	-10.1960	-10.1917
HOMO+5	-10.2798	-10.2769	-10.2736	-10.2725

Table S6.3.1: Molecular orbital energy levels for different alkyl chains at the aglycone position.

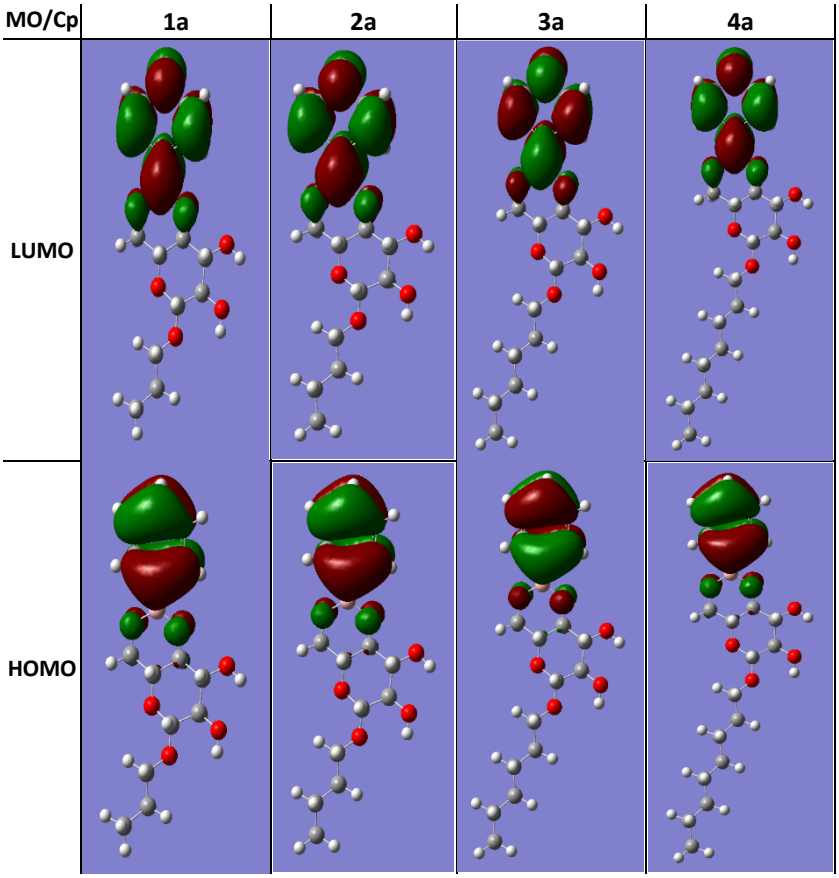

Figure S6.3.1: Representations of the frontier molecular orbitals for phenylboronates of glucosides with different alkyl chains at the aglycone position.

MO / Cp	2a	2b	2c	2d	2e
LUMO+5	3.2509	3.2117	3.2865	3.0204	3.1586
LUMO+4	3.0522	3.0386	3.0865	2.9801	3.0098
LUMO+3	2.8525	2.8408	2.8890	2.8299	2.8414
LUMO+2	2.8280	2.8136	2.8596	2.7170	2.7848
LUMO+1	1.9137	2.0648	1.8977	2.1537	1.3393
LUMO	1.1507	1.1511	1.4617	1.4245	0.9211
HOMO	-8.7631	-8.4088	-7.9315	-8.2629	-9.2146
HOMO+1	-8.7816	-8.6866	-8.8243	-8.4458	-9.3223
HOMO+2	-9.4894	-9.4929	-9.4355	-9.5098	-9.5013
HOMO+3	-10.0461	-10.0728	-10.0026	-10.0662	-10.0205
HOMO+4	-10.2050	-10.2094	-10.1609	-10.2118	-10.2238
HOMO+5	-10.2769	-10.2679	-10.1900	-10.2502	-10.3811

Table S6.3.2: Molecular orbital energy levels for a *n*-butyl chain with different substituents (R1, R2, R3).

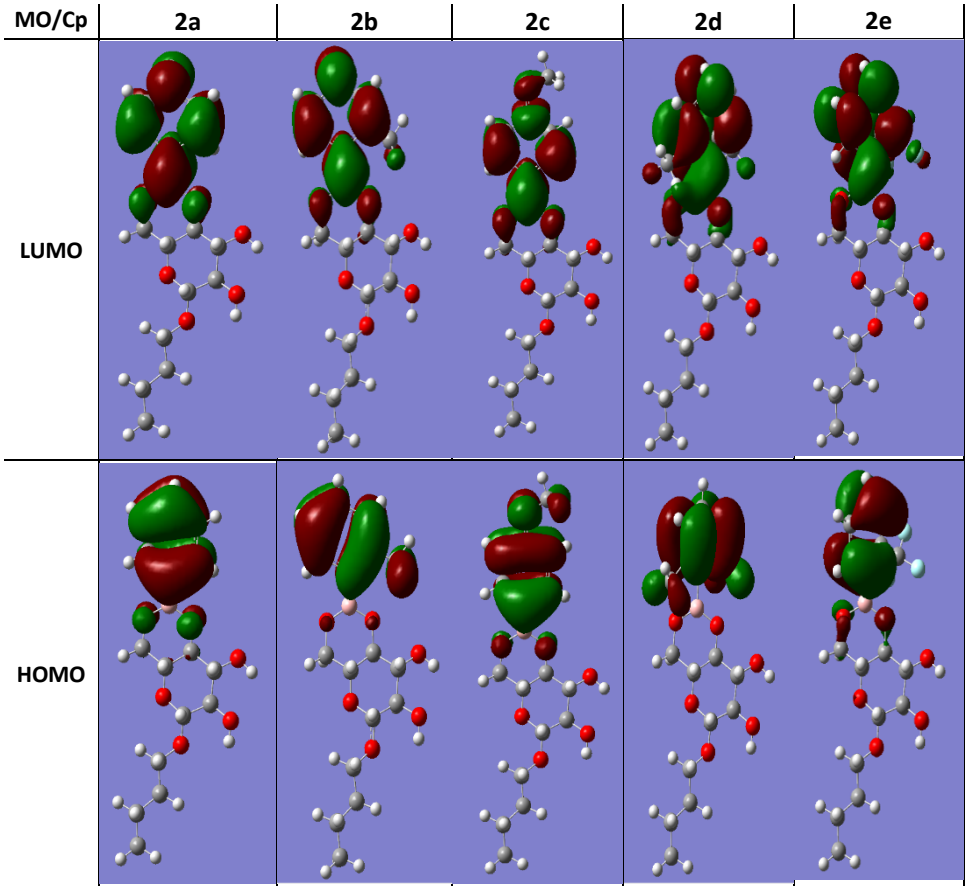

Figure S6.3.2: Representations of the frontier molecular orbitals for arylboronates butylglucosides with different aryl substituents (R1, R2, R3).

MO / Cp	4a	4b	4c	4d	4e
LUMO+5	3.1834	3.1788	3.2133	3.0030	3.1254
LUMO+4	3.0016	2.9894	3.0316	2.9633	2.9766
LUMO+3	2.8411	2.8291	2.8852	2.8199	2.8305
LUMO+2	2.8286	2.8169	2.8544	2.7224	2.7869
LUMO+1	1.9165	2.0677	1.9048	2.1581	1.3412
LUMO	1.1537	1.1554	1.4604	1.4196	0.9233
HOMO	-8.7607	-8.4055	-7.9312	-8.2605	-9.2124
HOMO+1	-8.7792	-8.6834	-8.8197	-8.4436	-9.3198
HOMO+2	-9.4831	-9.4869	-9.4238	-9.5030	-9.4951
HOMO+3	-10.0390	-10.0657	-9.9846	-10.0594	-10.0143
HOMO+4	-10.1917	-10.1972	-10.1454	-10.2004	-10.2105
HOMO+5	-10.2725	-10.2643	-10.1846	-10.2431	-10.3756

Table S6.3.3: Molecular orbital energy levels for a n-octyl chain with different aryl substituents (R1, R2, R3).

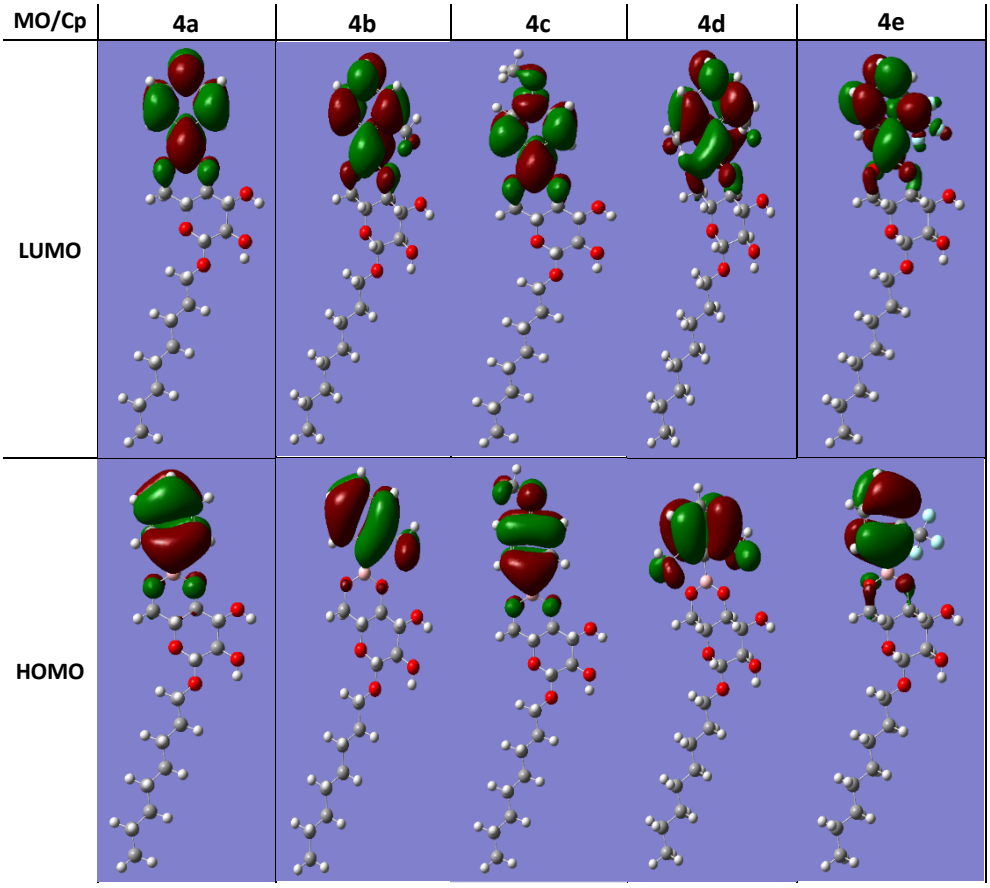

Figure S3.3: Representations of the frontier molecular orbitals for arylboronates octylglucosides with different aryl substituents (R1, R2, R3).

S6.4 - Supporting references

[1] N. Shimada, S. Urata, K. Fukuhara, T. Tsuneda, K. Makino **2018**, 2.6-Bis(trifluoromethyl)phenylboronic Esters as Protective Groups for Diols: A Protection/Deprotection Protocol for Use under Mild Conditions, *Org. Lett.* ***20***, 6064−6068.

[2] L. Legentil. Y. Cabezas. O. Tasseau. C. Tellier. F. Daligault. V. Ferrières **2017**, Regioselective Galactofuranosylation for the Synthesis of Disaccharide Patterns Found in Pathogenic Microorganisms, *J. Org. Chem.* ***82***, 7114−7122.

[3] (a) I. D. I. Ramaite. T. van Ree **2017**, Computational Studies of Substituted Phenylboronic Acids in Common Electrolyte Solvents, *Arab. J. Sci. Eng.* ***42***, 4227-4238 ; (b) A. W. Bebeda. T. van Ree **2015,** Conformational Preferences and Electrochemical Performance of Ethyleneoxy Phenylboronate Electrolyte Additives, *Arab. J. Sci. Eng.* ***40***, 2841–2851.

[4] M. Tanaka, A. Nakagawa, N. Nishi, K. Iijima, R. Sawa, D. Takahashi, K. Toshima **2018**, Boronic-Acid-Catalyzed Regioselective and 1.2-cis-Stereoselective Glycosylation of Unprotected Sugar Acceptors via SNi-Type Mechanism, *J. Am. Chem. Soc*. ***140***, 3644−3651.

[5] S. Wan. J. Guo. J. Kim. H. Ihee. D. Jiang **2009**, A Belt-Shaped. Blue Luminescent. and Semiconducting Covalent Organic Framework, *Angew. Chem. Int. Ed*. ***47***, 8826–8830.

[6] E. Borowska, K. Durka, S. Lulinski, J. Serwatowski, K. Wozniak **2012**, On the Directing Effect of Boronate Groups in the Lithiation of Boronated Thiophenes, *Eur. J. Org. Chem.* ***2012***, 2208–2218.

[7] C. Vahlberg, M. Linares, P. Norman, K. Uvdal **2012**, Phenylboronic Ester- and Phenylboronic Acid-Terminated Alkanethiols on Gold Surfaces, *J. Phys. Chem. C* ***116***, 796–806.

[8] J. N. Bentley, S. A. Simoes, E. Pradhan, T. Zeng, C. B. Caputo **2021**, The synthesis, properties, and reactivity of Lewis acidic aminoboranes, *Org. Biomol. Chem*. ***19***, 4796–4802.

[9] P. Pacholak. K. Gontarczyk. Radosław Kaminski. Krzysztof Durka. S. Lulinsi **2020**, Boronate Covalent and Hybrid Organic Frameworks Featuring PIII and P=O Lewis Base Sites, *Chem. Eur. J.* 26. 12758 – 12768.

[10] A. J. Cardenas-Valenzuela, J. Baldenebro-Lopez, J. A. Guerrero-Alvarez, H. Höpfl, D. Glossman-Mitnik, J. J. Campos-Gaxiolaa, A. Cruz-Enriquez **2018**, Supramolecular arrangement and photophysical properties of a dinuclear cyanophenylboronic acid ester, *Acta Cryst.* ***C74***, 452–459.

[11] H. Li, H. Li, Q. Dai. H. Li, J.-L. Brédas **2018***,* Hydrolytic Stability of Boronate Ester-Linked Covalent Organic Frameworks. *Adv. Theory Simul.* ***1***, 1700015, 1-9.

[12] K. J. Donald, U. R. Gaillard, N. Walker **2022**, On Neutral Unsaturated Ouroboric Borylenes, *J. Phys. Chem. A,* ***126***, 5173-5185.

S7. Gelation data in Hansen space

Graph were plotted following the methodology of Bouteiller *et al. Soft Matter* **2018**, *14*, 4805-4809. doi:10.1039/C8SM00562A.

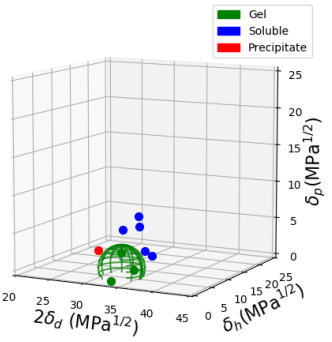

Gelation data in Hansen space for **2a**

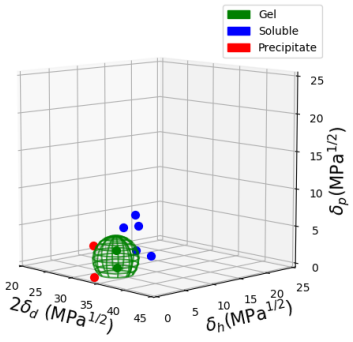

Gelation data in Hansen space for **4a**

S8. 1H NMR at variable temperature

S8.1. Variable temperature ^{1}H NMR of gel in toluene-d8 with **2a** (25°C, 30°C, 40°C, 50°C, 60°C, 70°C, 80°C, from bottom to top).

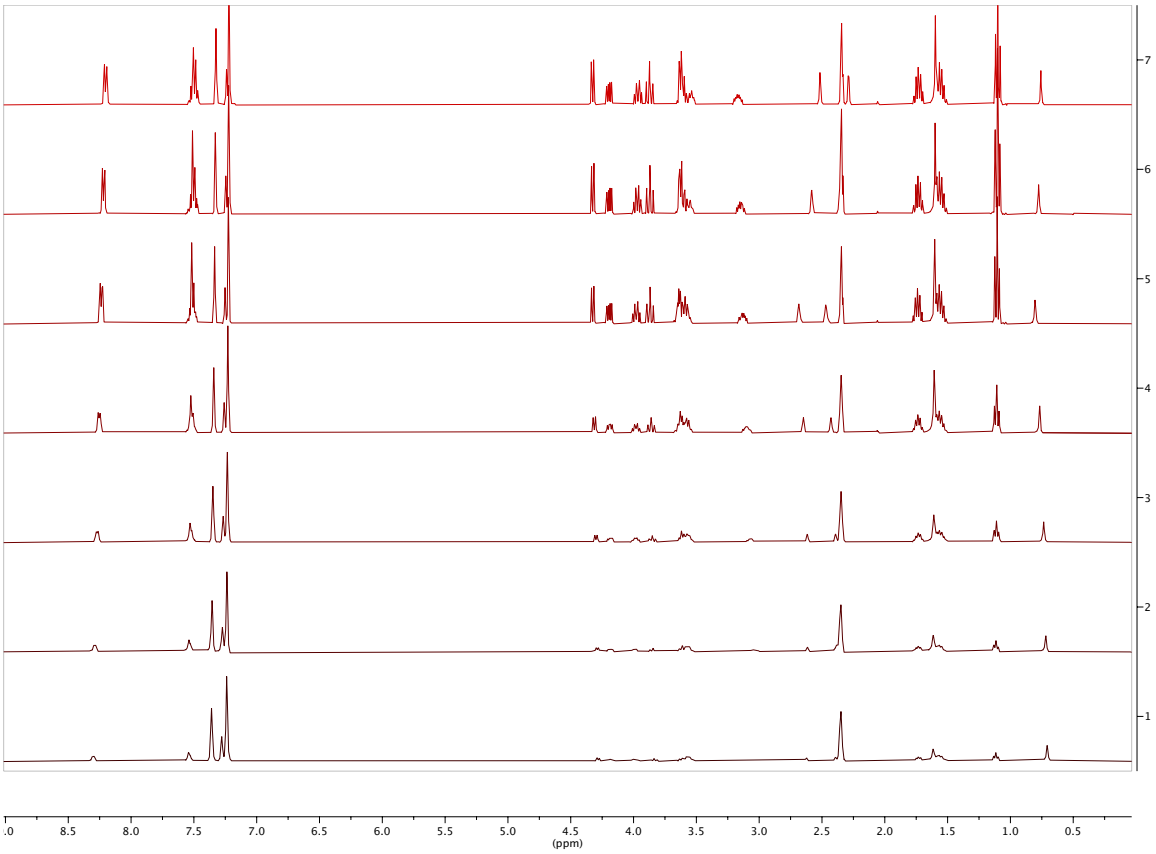

S8.2. Variable temperature ^{1}H NMR of gel in toluene-d8 with **3a** (25°C, 30°C, 40°C, 50°C, 60°C, 70°C, 80°C, from bottom to top).

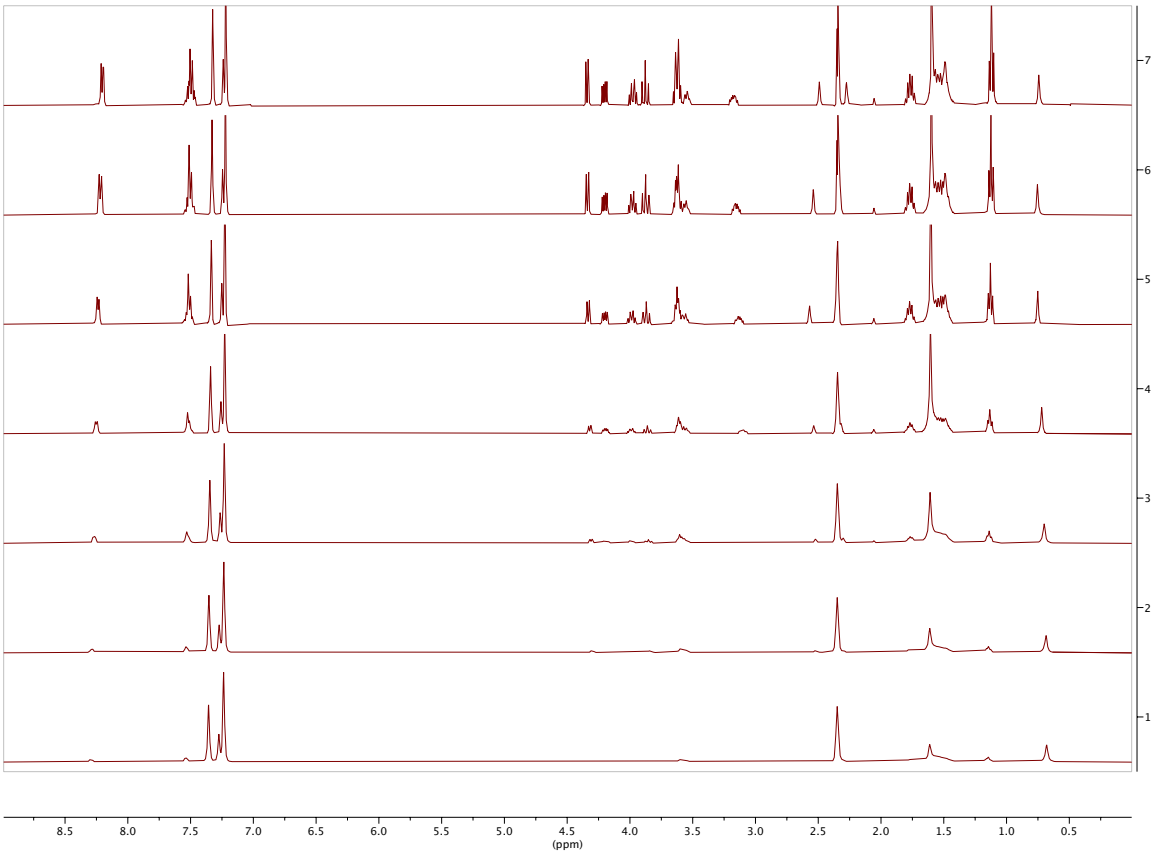

S8.3. Variable temperature ^{1}H NMR of gel in toluene-d8 with **4a** (25°C, 30°C, 40°C, 50°C, 60°C, 70°C, 80°C, from bottom to top).